crystals

MDPI

*Review*

# Supramolecular Arrangement and Conformational and Dynamic Properties of Chiral Smectic Liquid Crystals Obtained through Nuclear Magnetic Resonance: A Brief Review

**Valentina Domenici**

Dipartimento di Chimica e Chimica Industriale, Università di Pisa, Via Moruzzi 13, 56124 Pisa, Italy; valentina.domenici@unipi.it; Tel.: +39-050-2219-215/267

**Abstract:** Ferroelectric and antiferroelectric smectic liquid crystalline (LC) phases are still at the center of investigations and interests for both their fundamental properties and variety of technological applications. This review aims to report the main contributions based on different nuclear magnetic resonance (NMR) techniques to the study of chiral liquid crystalline calamitic mesogens forming smectic phases, such as the SmA, the SmC* (ferroelectric), and the $SmC^*_A$ (antiferroelectric) phases. $^2H$ NMR and $^{13}C$ NMR techniques and their combination were of help in clarifying the local orientational properties (i.e., the molecular and fragments' main orientational order parameters) at the transition between the SmA and the SmC* phases, and in the particular case of de Vries liquid crystals, NMR studies gave important clues regarding the actual models describing the molecular arrangement in these two phases formed by de Vries LCs. Moreover, this review describes how the combination of $^2H$ NMR relaxation times' analysis, $^1H$ NMR relaxometry, and $^1H$ NMR diffusometry was successfully applied to the study of chiral smectogens forming the SmC* and $SmC^*_A$ phases, with the determination of relevant parameters describing both rotational molecular and internal motions, collective dynamics, and translational self-diffusion motions. Several cases will be reported concerning NMR investigations of chiral ferroelectric and antiferroelectric phases, underlining the great potential of combined NMR approaches to the study of supramolecular, conformational, and dynamic properties of liquid crystals.

**Keywords:** ferroelectric liquid crystals; orientational order; de Vries liquid crystals; orthoconic liquid crystals; antiferroelectric liquid crystals; dynamic motions; conformational properties



**Citation:** Domenici, V. Supramolecular Arrangement and Conformational and Dynamic Properties of Chiral Smectic Liquid Crystals Obtained through Nuclear Magnetic Resonance: A Brief Review. *Crystals* **2024**, *14*, 823. https://doi.org/10.3390/cryst14090823

Academic Editor: Vladimir Chigrinov

Received: 26 August 2024
Revised: 16 September 2024
Accepted: 17 September 2024
Published: 20 September 2024



## 1. Introduction

Since their discovery by Meyer et al. in 1975 [1], ferroelectric liquid crystals (LCs) have attracted the attention of both the scientific community and the industry up to the present day. The first ferroelectric liquid crystals were chiral mesogens with the typical rod-like shape (i.e., calamitic LCs) forming smectic phases [1–4]. As reported by Goodby [4], the molecular chirality induces new liquid crystalline phases, with a supramolecular structure characterized by a helical arrangement of molecules. Molecular chirality thus induces local structural asymmetries, which reflect the peculiar organization of LC molecules in the different mesophases [5]. The ferroelectric smectic phase, called the SmC* phase, is analogous to the achiral SmC phase, where the local phase director, ***n***, is tilted by an average tilt angle $\theta$ with respect to the normal layer. In the case of the achiral SmC phase, the symmetry of the phase is $C_{2h}$, with a two-fold axis, a mirror plane, and a center of inversion as symmetry elements (see the representation in Scheme 1a). In the SmC* phase, the presence of chiral molecules (right- or left-handed ones) breaks the symmetry, and the only symmetry element is the $C_2$ axis, thus reducing the symmetry of the phase from $C_{2h}$ to $C_2$. This symmetry property is at the origin of several peculiar properties of the SmC* phase, such as the ferroelectricity [1–4,6,7]; in fact, each smectic layer has a spontaneous polarization, *Ps*. As shown in Scheme 1b, the supramolecular helical distribution

of the phase director corresponds to an analogous distribution for the spontaneous polarization along the helical axis (see the light blue arrows). Within a helical pitch, the polarization averages to zero. However, if an electric field, E, is applied perpendicularly to the helical axis, a net macroscopic polarization is observed due to the unwinding of the helix. This phenomenon is at the basis of several technological applications of the SmC* phase [1–4,7–9], such as the ferroelectric liquid crystal displays based on the surface-stabilized ferroelectric liquid crystals (SSFLCs) [8,9].

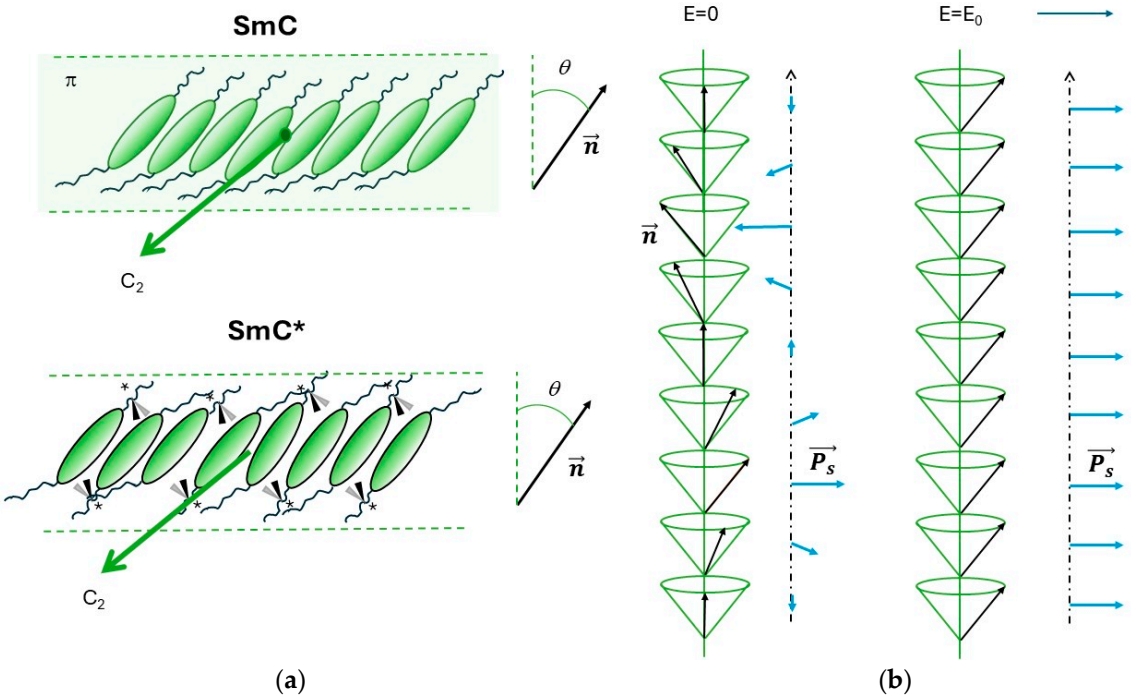


**Scheme 1.** (**a**) Top: achiral molecules in an SmC layer. The mirror plane, the two-fold rotational axis, and the center of inversion are drawn. Bottom: chiral molecules in an SmC* phase. Note that the asterisks stay for chiral carbon center. The two-fold rotational axis is drawn. In both cases, the phase director, **n**, is tilted with respect to the normal layer by the tilt angle, θ. (**b**) On the left: helical distribution of the phase director (black arrows) and of the spontaneous polarization (light blue arrows) in the SmC* phase. On the right: orientation of the phase director and spontaneous polarization when an electric field is applied perpendicularly to the helical axis.

Ferroelectric liquid crystal displays (FLCDs) present several advantages [7–9] with respect to the twisted nematic liquid crystal displays (TNLCDs), which are commonly used in digital devices and display technology. For instance, the switching time, τ, which is the characteristic time of reorientation of the LC phase from the on and the off states, is much smaller in FLCDs than in TNLCDs.

The study of new chiral LC molecules with a high molecular dipole led to the discovery of another type of chiral smectic phase in 1989 by Chandani et al. [10]: the antiferroelectric or anticlinic smectic phase, called the $SmC^*_A$ phase. In the antiferroelectric smectic phase, the phase director, **n**, the tilt angle, $\theta$, and the in-layer spontaneous polarization, *Ps*, change their sign and orientation from one layer to another (see Scheme 2). If two consecutive smectic layers are considered, the total polarization is zero. On a larger scale, the supramolecular structure of the $SmC^*_A$ phase results from the superposition of two helices shifted by a half pitch. It is worth noticing that there is not an analogue to the $SmC^*_A$ phase for achiral LCs. The interest in the $SmC^*_A$ phase is related to the electro-optical behavior and its potential positive impact on the display technology [11–16]. Antiferroelectric smectic phases are typically characterized by a tilt angle, θ, larger than the ferroelectric smectic phases: 25–30° vs. 22–23° [13]. Despite intense studies, the molecular origin of the antiferroelectric smectic

phase is still unknown. Moreover, so far, there are no commercial displays based on antiferroelectric liquid crystals [13]. Several technical problems, such as the presence of defects at the display surface and a substantial lack of reproducibility after many operating cycles, have limited the applications of antiferroelectric LCs, but, at the same time, they have stimulated the search for new LC materials.

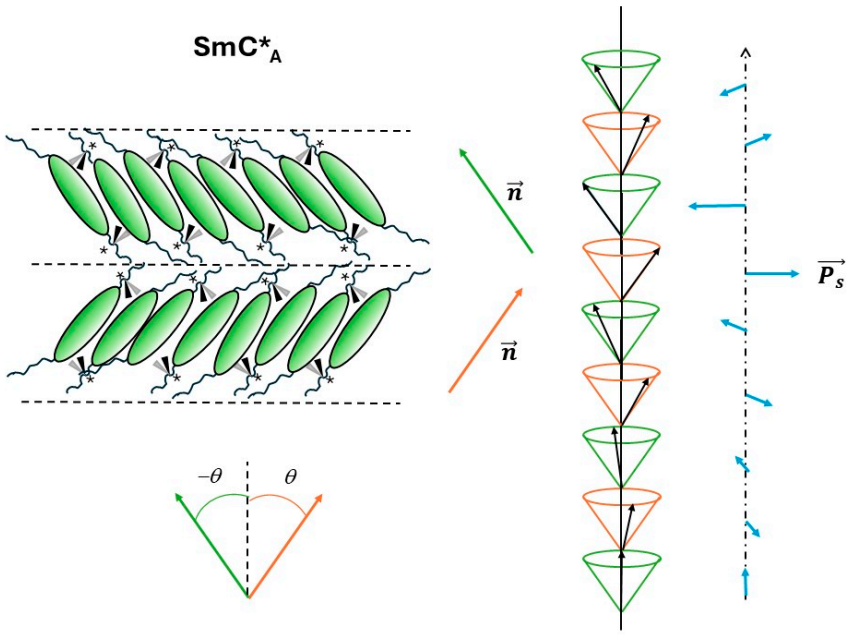


**Scheme 2.** On the left: two consecutive layers in the SmC*$_A$ phase. The orientation of the phase director for the two smectic layers is drawn. The tilt angle in the two consecutive layers changes signs. On the right: representation of the two helices superimposed (drawn in orange and green colors) with the distribution of the phase director (black arrows) and the spontaneous polarization (light blue arrows) in the SmC*$_A$ phase.

Among the interesting new chiral liquid crystalline materials, a new class of fluorinated smectic liquid crystals, namely the orthoconic antiferroelectric liquid crystals [13,17–21], was designed as pure compounds or as mixtures of different compounds. These materials typically show both the SmC* and the SmC*$_A$ phases. The antiferroelectric phase formed by the orthoconic liquid crystals is of particular interest for display technology. In fact, these LC systems have an average tilt angle of about 45°; a tilt angle in the range between 42° and 47° is considered optimal to guarantee the black state and to improve the display's performance [13]. In the last two years, several papers have been published concerning the relationship between the molecular structural features, the appearance of highly tilted smectic phases, and their peculiar electro-optic properties [22–26].

Another class of chiral smectogens of great interest for technological applications is that of de Vries LC compounds [27–31]. These chiral molecules may organize to form both the SmA (untilted phase) and the SmC* phase. Their main feature is related to the behavior at the SmA-SmC* transition, which is usually associated with layer shrinking when molecules pass from an untilted smectic phase to a tilted smectic phase. In the case of de Vries LCs, however, the observed shrinking is very small (less than 5%) [28,29]. Several models have been proposed to explain this phenomenon, and still the research in this field is ongoing. The interest in these systems is indeed related to the possibility to solve one of the main problems in FLCDs: the formation of 'Chevron'-like defects at the surface of the display as a consequence of the layer shrinkage from the SmA to the SmC* layers' arrangement. It is worth noticing that the ferroelectric and antiferroelectric phases can be formed by a particular class of achiral molecules, called banana-shaped or bent-shaped liquid crystals [32–35], too. Moreover, in recent years, a new type of ferroelectric phase,

having an orientational order but not a positional order, was discovered, which is formed by chiral molecules with very high polarity: the ferroelectric nematic phase [36–40].

Most of the applications of ferroelectric and antiferroelectric smectic phases are related to display technology, as previously mentioned, and the research in this field is still very active, as demonstrated by recent papers concerning the optimization of parameters for fast optical switching [41] and in-plane electro-optical switching [42]. Moreover, other recent studies have explored new applications in the field of tunable circular devices [43], wrinkled surfaces for soft matter biomimetics [44], and optical imaging devices [45].

This review will present some of the main results obtained by means of nuclear magnetic resonance (NMR) [46–52] concerning the SmA, SmC*, and SmC*$_A$ phases formed by chiral rod-like liquid crystals, focusing on molecular, supramolecular, and dynamic properties. For simplicity, in this review, the technical aspects related to the NMR experiments, such as optimized parameters and sample preparations, are not reported, as these details are reported in previous papers and reviews. The aim of the present review is to provide a state of the art of the NMR investigations performed on these particular mesophases and to underline the potential of NMR techniques, such as $^2$H NMR, $^{13}$C NMR static techniques, $^1$H NMR relaxometry, and $^1$H NMR diffusometry, for understanding key properties in new liquid crystalline phases.

## 2. The SmA Phase of Chiral Calamitic Liquid Crystals Studied through NMR

### *2.1. Ordering Properties and Supramolecular Structure of $^2$H NMR*

The first NMR studies applied to the field of liquid crystals [53,54] were based on the $^2$H nucleus, which is a quadrupolar magnetic nucleus with low sensitivity due to the low natural isotopic abundance. However, if the molecular systems are selectively deuterated, with percentages usually close to 100%, $^2$H NMR becomes a very powerful spectroscopic technique able to probe local properties, such as conformational, orientational, and dynamic ones [47–49,52]. The first $^2$H NMR investigations were focused on achiral liquid crystalline mesogens, forming the nematic and the SmA phases [55,56]. In the last thirty years, however, several studies have been devoted to the NMR investigation of chiral LC molecules and their molecular and supramolecular properties, including, in particular, their smectic phases, as reviewed by Domenici et al. [57]. As an example, the case of two optically pure isotopomers of the compound 4-[4′-(1-methyl heptyloxy)] biphenyl 4-(10-undecenyloxy) benzoate (**11EB1M7**) deuterated selectively on the phenyl and biphenyl fragments (see Scheme 3) is here reported [58]. The interest in this smectogen was related to the fact that it presents a rich variety of chiral mesophases (I 115.2 °C BPI 114.8 °C N* 112.8 °C TGBA* 107.0 °C SmA 100.0 °C SmC* 78.0 °C SmI* 73.8 °C Cr) and that it was the precursor of a ferroelectric side-chain liquid crystalline polymer [59]. As shown in Scheme 3, chiral molecules are arranged in the SmA phase with their molecular long axis, z, aligned, on average, parallel to the phase director, $\vec{n}$, and perpendicular to the smectic layers. In this sense, no differences can be observed between a chiral SmA phase and an achiral SmA phase from the NMR experimental point of view. In fact, when the LC sample is inserted into the NMR magnetic field, the director of the SmA phase, formed by calamitic liquid crystals with a rigid aromatic core, similarly to the **11EB1M7** sample, orients parallel to the external magnetic field, thus giving a macroscopic uniaxial orientation to the whole LC sample.

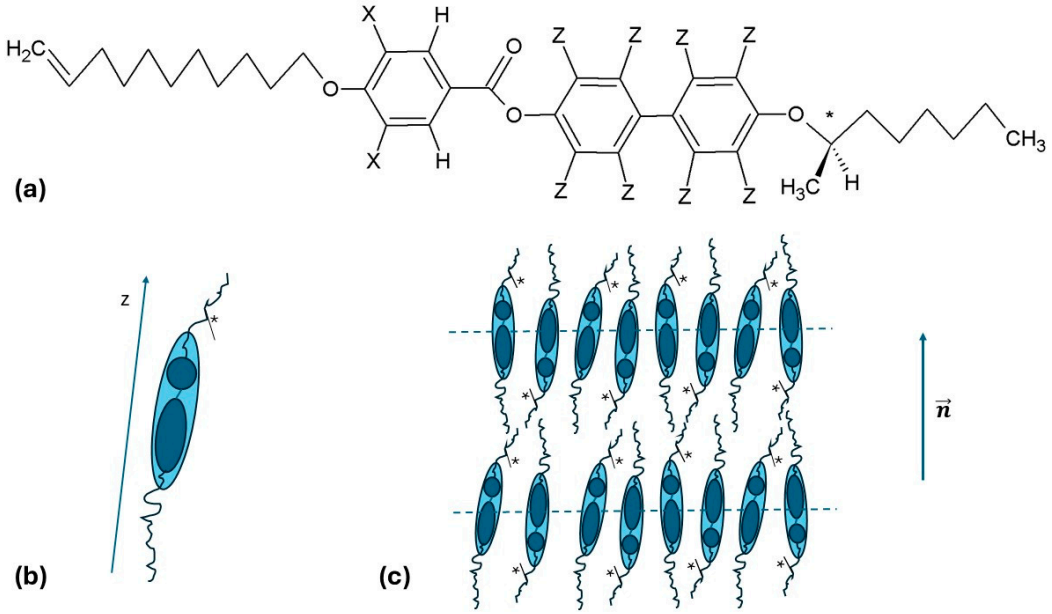


**Scheme 3.** (**a**) Molecular structure of two selectively $^2$H-labeled isotopomers of the liquid crystal called **11EB1M7**: **11EB1M7-d$_2$** (X = $^2$H, Z = $^1$H) and **11EB1M7-d$_8$** (X = $^1$H, Z = $^2$H). (**b**) Representation of the molecule composed of the aromatic core and the two lateral chains (achiral and chiral ones); the long molecular axis, z, is also shown. (**c**) Molecular arrangement in the SmA phase (two consecutive layers are shown); the periodicity of the mass centers is indicated through dashed lines, and the director vector, $\vec{n}$, is shown.

As a consequence of this macroscopic orientation, $^2$H NMR spectra in the SmA phase are relatively simple, as for each type of deuteron the signal is characterized by a large doublet due to the quadrupolar interaction, which can be further split, in the simplest case, into a small doublet if the $^2$H nucleus is coupled with a $^1$H. This simplest case is observed for the **11EB1M7-d$_2$** mesogen, deuterium labeled on the phenyl ring, and an example of experimental and calculated $^2$H NMR spectra recorded at 7.05 T is shown in Figure 1a,c, respectively [58].

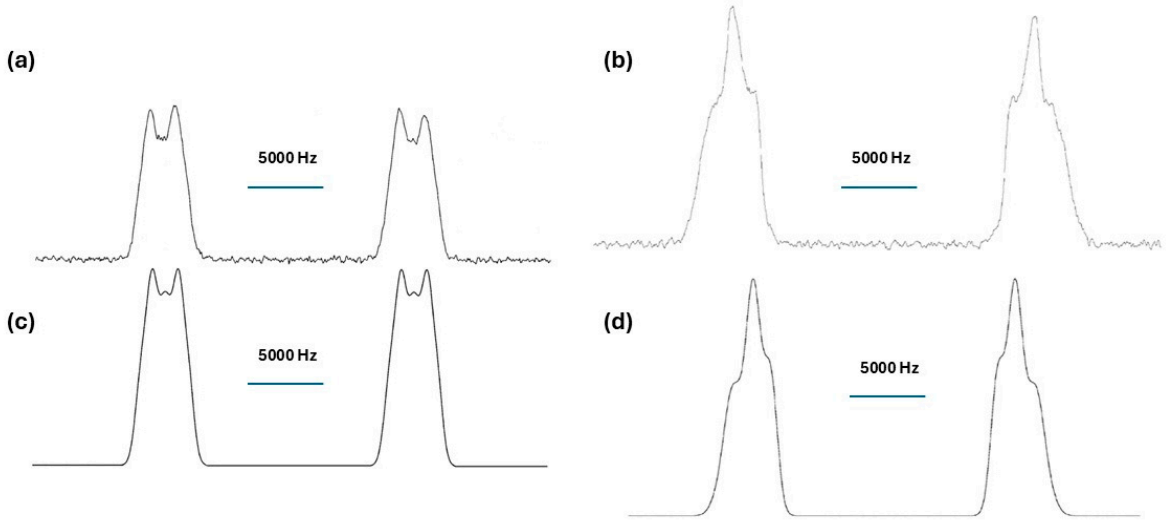


**Figure 1.** $^2$H NMR experimental spectra, (**a**,**b**), and $^2$H NMR simulated spectra, (**c**,**d**), of the smectogen **11EB1M7-d$_2$**, (**a**,**c**), and of the smectogen **11EB1M7-d$_8$**, (**b**,**d**), at 98 °C in the SmA phase. Spectra were acquired without proton decoupling. Experimental details are reported in ref. [58]. Reproduced with permission from [58]. Copyright © 2003 American Chemical Society.

The experimental $^2$H NMR spectrum (see Figure 1b) observed for the **11EB1M7-d$_8$** mesogen, deuterium labeled on the biphenyl moiety, presents a more complex shape due to the presence of four not-equivalent deuterons, which have different quadrupolar splittings, $\Delta\nu_q^i$, superimposed to various $^2$H-$^1$H dipolar splittings, $\Delta\nu_D^{ij}$, as demonstrated by the simulation (see the simulated $^2$H NMR spectrum in Figure 1d). The analysis of the T-dependence of the quadrupolar and dipolar splittings allows for accessing the local orientational order properties of the LC mesogens and, in particular, determining several Saupe orientational order parameters, such as the main orientational order, $S_{zz}$, and the biaxiality, $S_{yy}$-$S_{xx}$, which are usually referred to as the deuterated moiety. $^2$H NMR spectroscopy is indeed a technique able to probe local molecular properties, and in case of the availability of more than one selectively deuterated isotopomer, this means there is a possibility to 'observe' different sites of the LC molecule [55,56].

In the case of the **11EB1M7** smectogen, the main orientational order parameters, $S_{zz}$, for the two aromatic components of the rigid core can be obtained from the analysis of $^2$H NMR spectra and their temperature behavior in the SmA, SmC*, and SmI* phases, as shown in Figure 2. Focusing on the SmA phase, the **11EB1M7** smectogen shows the typical trend of the main orientational order parameter, which increases by decreasing the temperature, remaining in the range of 0.6 to 0.75, which is rather typical of the SmA phase [47,49,57,60]. In addition, it is clear from Figure 2 that the two moieties, the phenyl and the biphenyl ones, experience a different value of the main order parameter, thus reflecting a different average orientation with respect to the phase director. As reported in ref. [58], by following the temperature behavior of these two local order parameters in the whole mesophasic temperature range, it is possible to observe a change in the average conformation and orientational properties of the LC core when passing from the SmA to the SmC* and from the SmC* to the highly ordered SmI* phase. This will be further commented on in the next section.

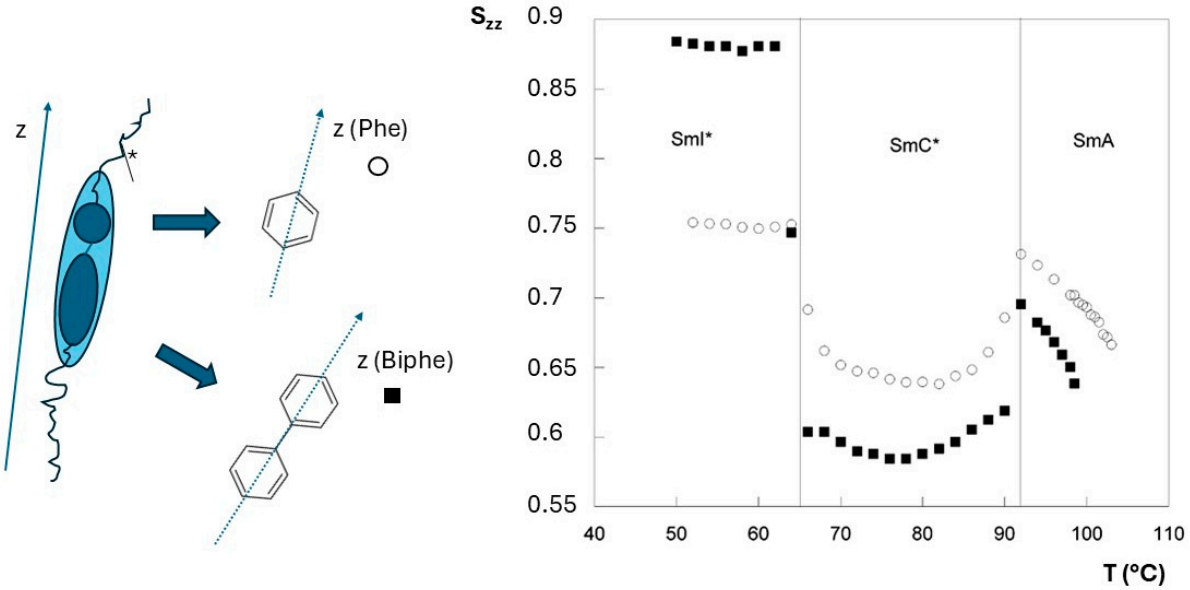


**Figure 2.** Trend of the orientational order parameters $S_{zz}$, referring to the phenyl (empty circles) and the biphenyl (full squares) fragments as a function of temperature (°C) in the SmA, SmC*, and SmI* phases obtained from the analysis of the $^2$H NMR spectra of the two samples, **11EB1M7-d$_2$** and **11EB1M7-d$_8$**. The orientation of the *z* axis of the phenyl ring and the biphenyl fragment, as well as the orientation of the long molecular axis of the LC molecule, are schematically drawn on the left. Note that the experimental error is smaller than the dimensions of the symbols. Reproduced with permission from [58]. Copyright © 2003 American Chemical Society.

The orientational ordering properties of the smectic A phase formed by chiral molecules was investigated by means of $^{13}$C NMR spectroscopy [61–63], too. As it will be shown

in Section 3, $^{13}C$ NMR techniques allow for the observation of all carbon sites of the LC molecule, with the disadvantage of a much more complex data analysis, which requires knowledge of the carbon chemical shift tensors, the use of several combined monodimensional $^{13}C$ and bi-dimensional $^{1}H$-$^{13}C$ NMR solid-state experiments, and/or the support of DFT computations [51,57,63–65]. In the case of the **11EB1M7** smectogen, for instance, the complete analysis of $^{13}C$ NMR data in terms of orientational order properties in the SmA phase was performed by fixing some of the parameters obtained from $^{2}H$ NMR [58].

### *2.2. Dynamic Properties of Liquid Crystals in the SmA Phase Obtained through NMR*

Information about the dynamic properties of liquid crystals in the SmA phase can be provided using several NMR methods [49,52,57]. Among them, the analysis of $^{2}H$ NMR relaxation times, spin–lattice ($T_1$) and spin–spin ($T_2$) relaxation times, in terms of specific molecular models was revealed to be successful in describing the main dynamic contributions in the 100 KHz–500 MHz frequency region. As an example, the $^{2}H$ quadrupolar ($T_{1Q}$) and Zeeman ($T_{1Z}$) spin–lattice relaxation times, which can be measured directly through a specific NMR sequence, can be related to the spectral density of motions. The availability of theoretical models specific to liquid crystals relating the spectral densities to relevant parameters for each type of motional process was fundamental in order to extract dynamic information from the experimental relaxation times. Without going into detail regarding these models and the procedure of data analysis, described, for instance, in [57], it is worth noticing that this approach has been used to obtain information from $T_{1Q}$ and $T_{1Z}$ spin–lattice relaxation times about several motions, such as 1. overall reorientations of the whole LC molecule, which can be assumed to behave as an ellipse with two main rotational diffusion coefficients, defined as $D_{//}$ (reorientation around the long molecular axis) and $D_{\perp}$ (reorientation around a perpendicular axis with respect to the long molecular axis) and 2. internal motions of molecular fragments described by an internal reorientation diffusion coefficient, $D_R$ (i.e., in the case of a selectively deuterated fragment, it describes the reorientation around the fragment's main axis). As an example, the temperature behavior of these rotational diffusion coefficients for the compound **11EB1M7** in the SmA phase obtained by analyzing $^{2}H$ NMR spin–lattice relaxation times measured at 7.05 T (46.04 MHz as deuterium Larmor frequency) is shown in Figure 3. Taking into account the schematic representation of LC molecules in the SmA phase reported in Scheme 1, we can imagine these molecules rotating quite quickly around their long molecular axis, with a $D_{//}$ of about 3–4 $\times$ $10^{-9}$ $s^{-1}$. From Figure 3, it is evident that the biphenyl fragment rotates a bit faster than the phenyl ring, but, as a general remark, the order of magnitude of the reorientation diffusion coefficient is the same for all of them [58]. Interestingly, the reorientation of the LC molecules around a perpendicular axis, namely the flip–flop motion, is not hindered, and it is just slower by an order of magnitude ($D_{\perp}$ of about 1–2 $\times$ $10^{-8}$ $s^{-1}$). So, we can imagine that LC molecules can rotate quite easily in these two directions when they are in the SmA phase. Moreover, as reported in the review by Cifelli et al. [48], because the slope of the temperature behavior is very similar, the activation energy for these reorientation motions is approximately the same, ranging from 20 to 45 kJ $mol^{-1}$ for similar smectogens.

The analysis of $^{2}H$ spin–spin ($T_2$) relaxation times is less common in smectic liquid crystals in terms of molecular motions. In principle, $^{2}H$ NMR $T_2$ are more sensitive to slow motional processes with respect to $^{2}H$ NMR $T_1$. In the SmA phase, there are other relevant motional processes in addition to the reorientation molecular and internal ones. For instance, SmA phases are usually characterized by a special type of collective motions, called layer undulations, due to the local fluctuations of a group of molecules around the phase director. These collective motions are typically active in the kHz frequency regime. Another important motional process present in the SmA phase is related to the translational self-diffusion, as molecules can indeed move in different directions within the smectic phase (in-plane diffusion) or in the perpendicular direction, passing from one

layer to another (transverse diffusion). Layer undulations and self-diffusion motions were investigated by means of $^1$H NMR relaxometry, which is a very useful technique because it can cover a wide frequency range, from few KHz to hundreds of MHz [66]. Few examples of applications of this technique have been published for chiral mesogens, giving rise to the relevant parameters describing these types of motional processes [67,68]. Detailed information about the anisotropy of the translational self-diffusion was obtained in the SmA phase by means of $^1$H NMR diffusiometry [69], which was very helpful in studying the behavior at the transition between different chiral smectic phases [70,71], as will be discussed in the next sections.

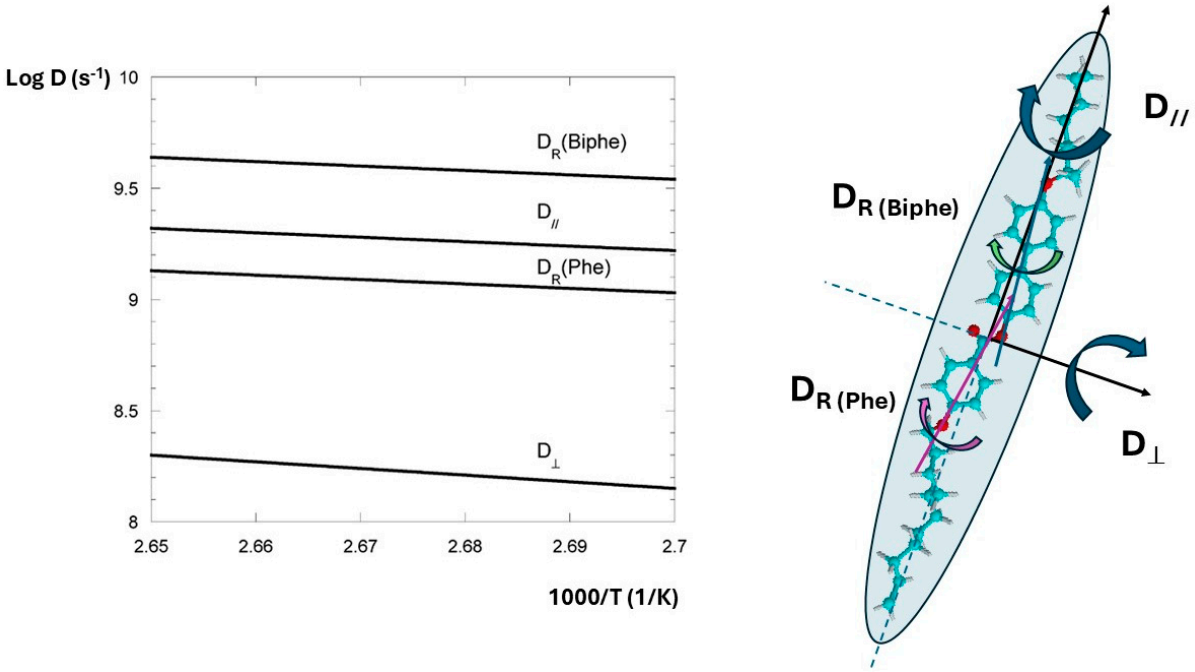


**Figure 3.** Logarithm of the diffusion constants $D_{//}$, $D_{\perp}$, $D_R$ (Phe), and $D_R$ (Biphe) ($s^{-1}$) vs. 1000/T (1/K) of the **11EB1M7** sample in the SmA phase, derived from the analysis of the $^2$H NMR spin–lattice relaxation times in terms of dynamic models (see the text for details). The four rotational motions are represented on the right. Reproduced with permission from [58]. Copyright © 2003 American Chemical Society.

## 3. The SmA–SmC* Phase Transition in Calamitic Liquid Crystals

The most interesting and probably the most studied smectic phase formed by chiral calamitic liquid crystals is the ferroelectric SmC* phase. The use of NMR spectroscopy has provided important contributions to understanding several molecular properties that are intimately related to physical properties of the SmC* phase. In the following paragraphs, the main results obtained through NMR investigations will be reviewed.

### *3.1. The Effect of the Magnetic Field on the Helical Supramolecular Structure of the SmC* Phase*

When an achiral tilted smectic phase, namely the SmC phase, is inserted into an external magnetic field, the local director, $\vec{n}$, and the LC molecules of each smectic layer tend to align parallel to the magnetic field (note that this is in the case of calamitic LCs having an aromatic core). This is due to the anisotropy of the molecular susceptibility, $\Delta\chi_m$, which is typically negative for rod-like liquid crystals with a core constituted by aromatic rings and positive for rod-like liquid crystals with a rigid core made by aliphatic cycles [72]. In the latter case, the alignment of LC molecules in the presence of the magnetic field is the opposite, as LC molecules align perpendicularly to the magnetic field. Meanwhile, in the case examined here, LC molecules tend to align parallel to the magnetic field in order to minimize the magnetic energy. As a consequence, the smectic layers tilt with

respect to the magnetic field, giving rise, at a macroscopic scale, to a V shape of the sample meniscus. This phenomenon can be explained in terms of the energy interaction between the smectic domains of LC molecules and the external magnetic field. In the case of an achiral smectogen forming both the SmA and the SmC phases, the main orientational order, as obtained, for instance, using the $^2$H NMR technique described in the previous section, increases by decreasing the temperature, with an eventual discontinuity in the slope passing from the SmA to the SmC phase [56]. A completely different behavior is observed in chiral smectogens at the SmA–SmC* transition [57–60]. In fact, the helical supramolecular structure of the SmC* domains (see, for instance, Scheme 1) is normally retained with the result that the helical axes align parallel to the magnetic field and LC molecules are titled with respect to the magnetic field as well as the local phase director, $\boldsymbol{n}$. As it will be shown, this macroscopic alignment of the SmC* phase in the presence of an external magnetic field results in an apparent decrease in the orientational order measured through NMR by decreasing the temperature [57–60]. The effect of the magnetic field on the supramolecular structure of the SmC* phase was first investigated by applying the magnetic field perpendicular to the helical axis, similarly to what was done to study the effect of the electric field [73]. However, in 1998, Zalar et al. [74] reported for the first time the phenomenon of helix unwinding and helix distortion by performing $^2$H NMR experiments at variable angles between the helical axes of the ferroelectric phases and the magnetic field. A few years later, $^2$H NMR investigations of a chiral smectogen at different magnetic field strengths [75] allowed us to study a new phenomenon, the unwinding of the helical distribution of the SmC* phase in the case of a magnetic field parallel to the helical axis above a critical value of the magnetic field.

In Figure 4, the orientation of the SmA, SmC*, and unwound SmC* (uSmC*) phases with respect to an external magnetic field, $B_0$, is represented.

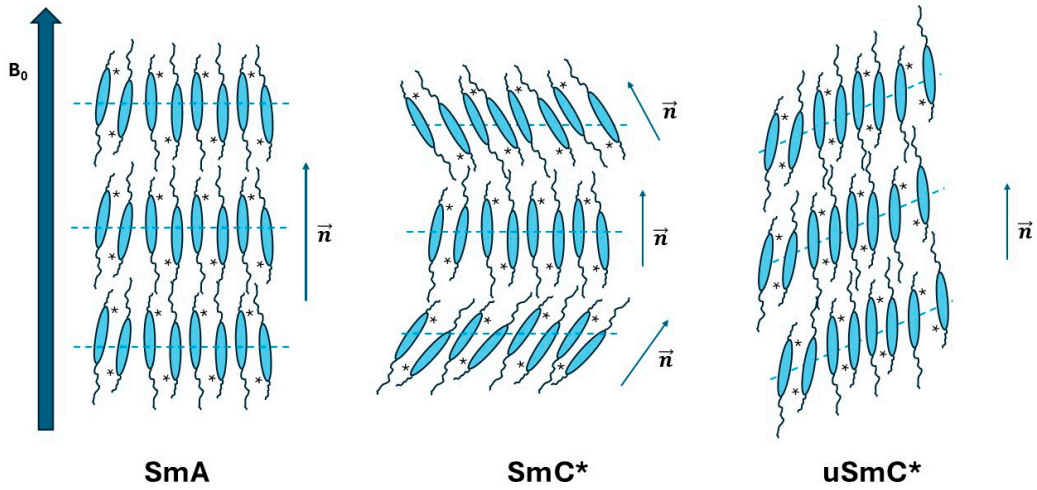


**Figure 4.** Representation of the molecular arrangement of chiral calamitic mesogens in the SmA, SmC*, and unwound SmC* (uSmC*) phases in the presence of an external magnetic field ($B_0$). Three consecutive layers are shown; dashed lines indicate the average distribution of the mass centers. The director vector, $\vec{n}$, is shown in the three cases. Note that in the SmC* phase, the supramolecular arrangement is helicoidal with the helical axis parallel to the external magnetic field.

Note that in the case of the SmC* phase, the helical distribution of directors is retained, while in the case of the uSmC* phase, the helical distribution is destroyed, the LC molecules and the local phase directors align parallel to the magnetic field, and the layers are tilted, similarly to what is observed in an achiral SmC phase. Later on, a similar behavior was observed for other smectogens, and a theoretical model based on the phenomenological Landau–de Gennes theory of phase transitions was developed [75,76]. The model allowed us to derive the expression of the energy density, $g$, for the SmA, SmC*, and uSmC* phases, thus introducing the energy contribution due to the interaction between the magnetic field

strength, $\boldsymbol{H}$, and the phase director, $\boldsymbol{n}$, namely $g_H = -(1/2)\Delta\chi_p(\boldsymbol{H}\cdot\boldsymbol{n})^2$ (where $\Delta\chi_p$ is the anisotropy of the magnetic susceptibility of the mesophase). From that, the theoretical expression of the temperature of the SmA–SmC*, SmA–uSmC*, and SmC*–uSmC* transitions can be computed, showing the strong dependence of the SmC*–uSmC* temperature transition based on the first term of the Landau–de Gennes model of the energy density (the 'a' coefficient), which is typical of each LC molecule, and other physical parameters, such as the elastic constants. Moreover, the critical field, $H_C$, which is necessary to unwind the helical axis, depends on the helical pitch, $p$, the elastic constant, $K$, and the anisotropy of the mesophase magnetic susceptibility, $\Delta\chi_p$: $H_C = \pi^2/p\sqrt{K/\Delta\chi_p}$. It is easy to check that the values of $H_C$ range between 5 and 20 T, depending on the specific LC smectogen [76]. An example of the temperature dependence of the energy density of these smectic phases and the temperature dependence of the main orientational order, S, computed using this model [76] is shown in Figure 5. The experimental values of $S_{zz}$ obtained from the analysis of $^2$H NMR spectra recorded at different magnetic field strengths (namely, 4.70 T, 7.05 T, and 9.39 T) for the smectogen **MBHB** are also shown in Figure 5 [76].

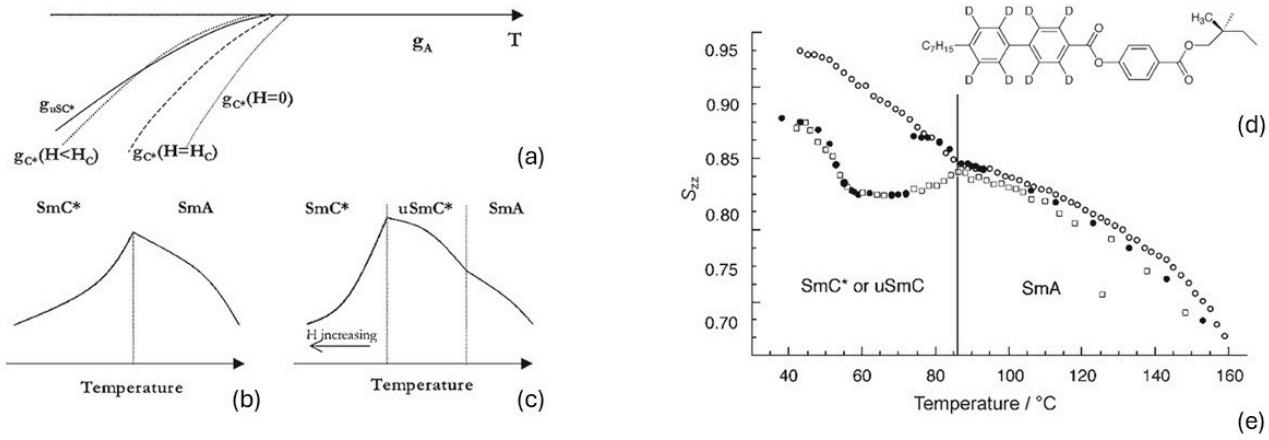


**Figure 5.** (**a**) Energy density, g, of the liquid crystalline system as a function of the temperature for three cases: (1) H = 0, (2) H = $H_C$, (3) H < $H_C$. Here, H is the magnetic field strength and $H_C$ is the critical value of the magnetic field strength (see the text). The energy densities, g, of the three phases are reported in bold (SmA), dashed (SmC*), and solid lines (uSmC*). (**b**,**c**) The main order parameter, S, as a function of the temperature of the SmA and SmC* phases (**b**) and the SmA, SmC*, and uSmC* phases (**c**), as obtained from the model proposed for the phase transitions. (**d**) Structure of the **MBHB-d$_8$** smectogen (deuterium labeled on the biphenyl fragment). (**e**) The main order parameter, S, of MBHB-d8 as a function of the temperature obtained by performing the $^2$H NMR study at different external magnetic fields: 4.70 T (empty squares), 7.05 T (full circles), and 9.39 T (empty circles). Note that the experimental error is smaller than the dimensions of the symbols. Reproduced with permission from [76]. Copyright © 2007 John Wiley & Sons, Inc.

These trends of the main orientational order $S_{zz}$ vs. the temperature from the SmA to the SmC* (or uSmC*) phases are very representative of what it is possible to observe when a chiral smectogen is investigated through NMR. In fact, if the operating NMR magnetic field is much lower than the critical field, the orientational order decreases by decreasing the temperature (see the empty squares in Figure 5e). This is due to the fact that the phase director, $\boldsymbol{n}$, is tilted and the tilt angle increases by decreasing the temperature. The observed decrease of the order parameter is indeed an apparent decrease [75,76]. If the external magnetic field is much higher than the critical magnetic field, the SmC* phase is totally unwound, and the orientational order continues increasing by decreasing the temperature at the phase transition (see empty circles in Figure 5e). In intermediate cases, when the magnetic field is close to the critical field, it is possible to observe a further phase transition from the uSmC* to the SmC* phase (see the full circles in Figure 5e). This temperature

transition is predictable using the theoretical model described above [76]. So far, this model has succeeded in explaining the behavior of several smectogens in the presence of external magnetic fields [60,76].

### *3.2. Order, Conformational Properties, and Dynamics of 'de Vries' Liquid Crystals*

As anticipated in the 'Introduction', a very interesting class of ferroelectric LCs is represented by the so-called 'de Vries' liquid crystals [27–31]. These smectogens have attracted the interest of the scientific community for their peculiar behavior at the transition between the SmA and the SmC* phases and for their electro-optical response in the SmA phase, such as the relatively strong electro-clinic effect [77–79]. Recent papers have been published reporting the synthesis of new types of 'de Vries' liquid crystals with fast electro-optic switching [80–82] and atomistic simulations on fluorinated 'de Vries' compounds aimed at exploring the structure–properties relationship [83]. NMR spectroscopy was very helpful in understanding crucial molecular properties of 'de Vries' smectogens, such as the conformational ones [7,84–90]. In the following paragraphs, the case of a 'de Vries' liquid crystal investigated through a multi-nuclei NMR approach is reported and commented on in view of the actual models proposed to explain the properties of 'de Vries' LCs.

#### 3.2.1. Order and Conformational Properties of 'de Vries' LCs Observed through NMR

The first $^2$H NMR study of a 'de Vries' liquid crystal was reported in 2010 [84]. The mesogen, called **9HL**, whose molecular structure is shown in Figure 6d, is a typical rod-like compound with a lateral chiral chain and a molecular core constituted by three aromatic rings connected through ester links. This compound was selectively deuterated on the first ring close to the achiral chain [84]. As seen for the smectogen **11EB1M7** and described in Section 2, $^2$H NMR spectra are relatively simple to interpret in terms of the local orientational order of the deuterated ring. In Figure 6a,b, the $^2$H NMR spectra of the **9HL-d$_2$** recorded in the presence of an external magnetic field of 7.05 T are reported. Both the quadrupolar and dipolar splittings increase by decreasing the temperature in the SmA phase, and they start decreasing at the SmC* phase transition. As described in the previous paragraph, this is the case of a magnetic field lower than the critical field for this smectogen, so the SmC* phase is not unwound by the magnetic field. Several additional experiments were performed at different values of the external magnetic field [85], and it was found that the critical field for the **9HL** sample is about 16.45 T. In Figure 6c, the values of the local orientational order relative to the para axis of the deuterated ring are reported as a function of the temperature for five different values of the operating NMR magnetic field, both in the SmA and in the SmC* phases. As it can be seen, at magnetic fields higher than the critical one, the SmC* phase is completely unwound. The values of $S_{zz}$ in the SmC* phase allowed us to calculate a relatively high tilt of the deuterated ring with respect to the magnetic field (reaching the highest value of 30° at low temperatures), and, interestingly, the values of $S_{zz}$ in the SmA phase, measured at different magnetic fields, indicate that even in the SmA phase, the deuterated ring is tilted, with an average tilt angle, θ, in the range of 5–12° [85]. From $^2$H NMR spectroscopy, we could confirm the peculiarity of this 'de Vries' compound, which presents an electro-clinic effect and small layer shrinking at the SmA–SmC* phase transition. However, the $^2$H NMR results added some new information at the molecular level, providing evidence of the need for a specific molecular model different from the simple 'random diffuse cone' model, which was first proposed to explain the properties of the SmA phase formed by de Vries [29]. $^2$H NMR results in the SmA phase are in agreement with the formation of local domains where LC molecules are aligned coherently, with the same tilt angle and azimuthal angle; for this reason, a new model, called the 'cluster diffuse cone', was proposed [84,85].

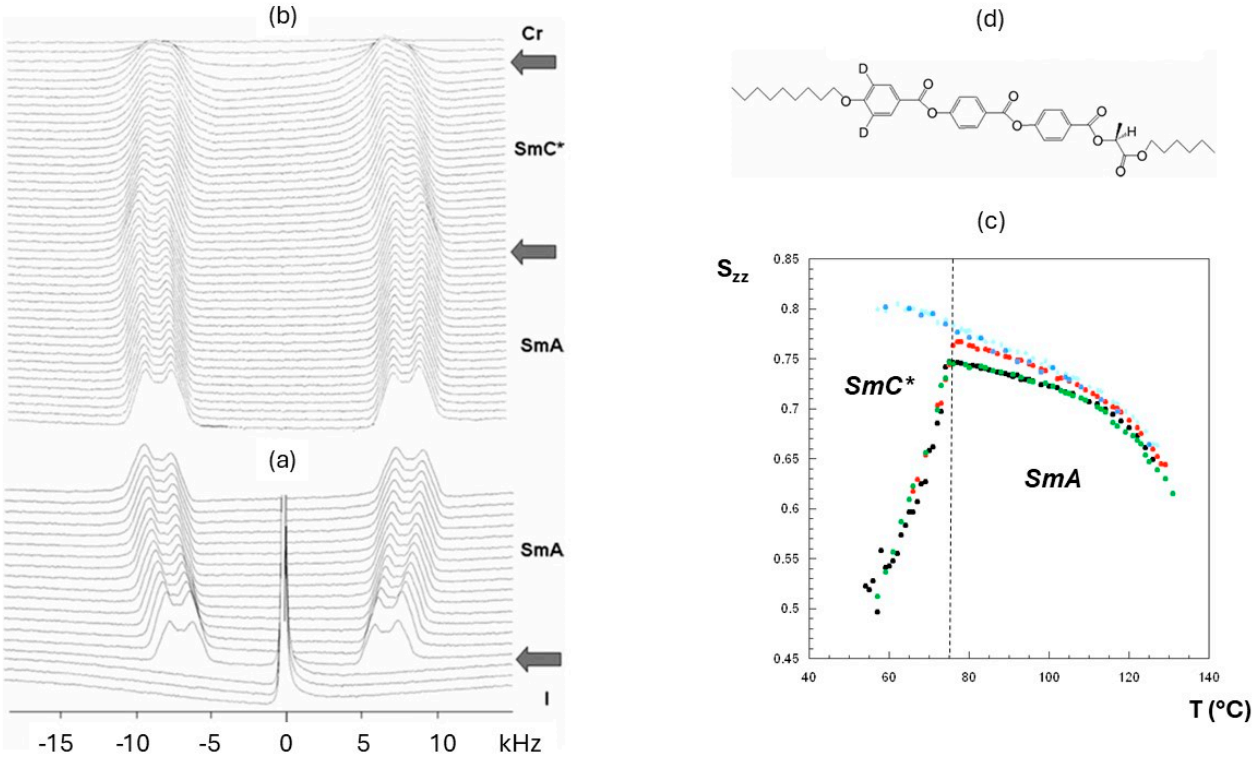


**Figure 6.** Stackplot of $^{2}$H NMR spectra of the **9HL-d$_2$** sample recorded at the magnetic field of 7.05 T without proton decoupling upon cooling the sample from the isotropic phase to the crystal phase. (**a**) Spectra from 132 °C to 96 °C every two degrees (from bottom to top). (**b**) Spectra from T = 95 °C to T = 45 °C every degree (from bottom to top). Mesophase transitions are indicated by a grey arrow. (**d**) Structure of the **9HL-d$_2$** sample (deuterium labeled on the phenyl ring closest to the achiral chain). (**c**) Temperature dependence of the order parameter $S_{zz}$ referring to the deuterated phenyl ring of the **9HL-d$_2$** sample, as obtained through the $^{2}$H NMR spectra analysis at different magnetic field strengths (4.25 T (green circles), 7.05 T (black circles), 11.75 T (red circles), 16.45 T (light blue circles), and 18.80 T (blue circles)). Note that the experimental error is less than the dimensions of the symbols. Reproduced and modified with permission from [84]. Copyright © 2010 John Wiley & Sons, Inc.

A way to go further in the understanding of the molecular properties of **9HL** at the SmA–SmC* phase transition was to perform a complete $^{13}$C NMR investigation [86]. Typical solid-state NMR techniques need to be applied in the case of liquid crystals. With respect to $^{2}$H NMR, $^{13}$C NMR allows us to see all not-equivalent carbons in the same spectrum; however, special care has to be taken in the assignment of all signals, and typically a series of complementary techniques are needed, such as the 1D $^{13}$C and 2D $^{1}$H-$^{13}$C HMBC and $^{1}$H-$^{13}$C HSQC experiments to assign the isotropic chemical shift for all carbon sites, and solid-state techniques, such as $^{13}$C CP NMR, $^{1}$H–$^{13}$C HETCOR, 2D PDLF, and 2D PASS experiments, to obtain the anisotropic contribution to the chemical shift and the chemical shift tensor elements. In the case of the **9HL** sample, all of these experiments were performed with the addition of further NMR experiments, such as the 2D $^{13}$C-$^{13}$C INADEQUATE experiment in the bulk isotropic phase and the $^{1}$H-$^{13}$C PDLF scaled dipolar couplings NMR experiment in the mesophases at different temperatures [86]. All experimental details are reported in ref. [86]. It is worth noticing that the analysis of the experimental chemical shift anisotropy as a function of the temperature for all carbon sites is more complex than the analysis of quadrupolar and dipolar splitting obtained through $^{2}$H NMR spectroscopy. In fact, the analysis is usually limited to the aromatic core of liquid crystals and rarely to the aliphatic carbons [46–49,51,52]. This approach has been applied to the study of **9HL** [86]. The assignment of almost all peaks in the $^{13}$C CP NMR spectrum recorded in the SmA phase is reported in Figure 7a,b. The position of these peaks

is related to both the isotropic, $\delta_{iso}$, and anisotropic chemical shift contributions, $\delta_{aniso}$, where the anisotropic chemical shift contribution depends on the local orientational order, which refers to the molecular fragment (i.e., $S_{zz}$ and $S_{yy}$-$S_{xx}$), and the 3D orientation of the chemical shift tensor, $\hat{\delta}$, and their principal values, $\delta_{ii}$.

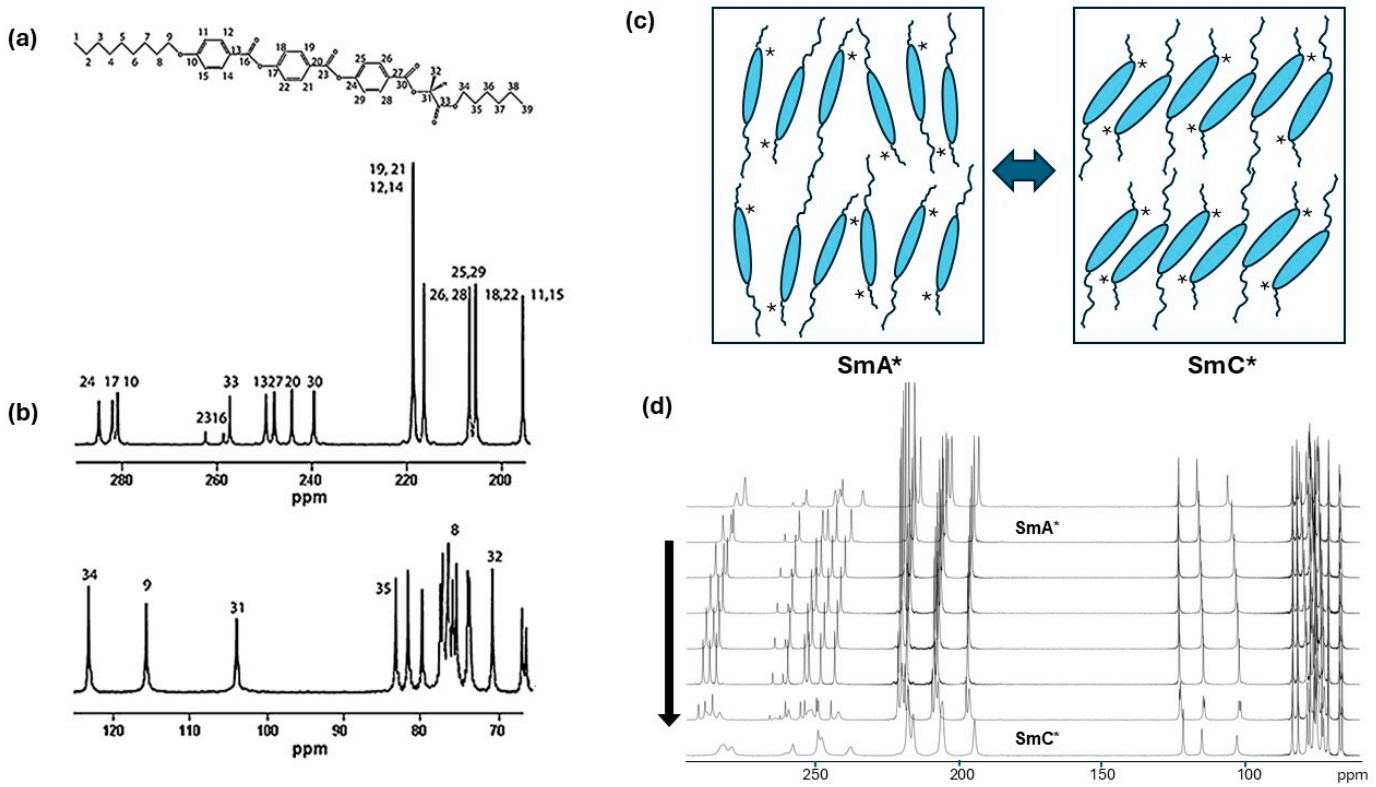


**Figure 7.** (**a**) Molecular structure of the **9HL** sample with all carbon sites numbered from 1 to 39. (**b**) Assignment of most of the carbon sites of the **9HL** sample of the static $^{13}$C CP NMR spectrum recorded in the SmA phase at T = 122 °C. (**c**) Representation of the molecular arrangement of the molecules of **9HL** in the SmA and in the SmC* phase, according to the model proposed in ref. [86]. (**d**) Stacked $^{13}$C CP NMR static spectra of the **9HL** sample acquired as a function of the temperature with an NMR instrument working at 9.46 T (temperatures decrease from top to bottom, as indicated by the black arrow). Figures are reproduced and modified with permission from [86]. Copyright © 2014 John Wiley & Sons, Inc.

The trend of the observed chemical shift ($\delta = \delta_{iso} + \delta_{aniso}$) for all carbon sites as a function of temperature for the **9HL** can be observed in Figure 7d. It is possible to note that the observed chemical shift of the signals ascribable to the aromatic and quaternary carbons (signals with δ higher than 180 ppm) increases in the SmA phase by decreasing the temperature; then, they start decreasing at the SmA–SmC* phase transition until the crystalline phase is reached due to the increasing tilt angle (see Figure 7c). On the contrary, the observed chemical shift of the signals ascribable to the aliphatic carbons (signals with δ smaller than 80 ppm) decreases in the SmA phase and increases in the SmC* phase. However, for these signals, the shift is much smaller due to the smaller chemical shift anisotropy, which is due to the combination of a small orientational order of the lateral chains and fast reorientation (internal) motions. The signals of the aliphatic alpha methylenoxy carbons (carbons 34, 9, and 31 in Figure 7a,b) have a different temperature behavior, as will be shown in Section 3.3.

The analysis of the chemical shift anisotropy of the aromatic core of ferroelectric liquid crystals has been reported for several other LC systems [7,46,51,57,61,64,90], and, in several cases, the chemical shift tensors were computed using DFT methods. In the case of **9HL**, the analysis of the chemical shift anisotropy for the three-ring core allowed for

the independent determination of the orientational order parameters of the three rings of **9HL** in the SmA phase, which was further supported by the independent analysis of the dipolar couplings obtained from the 2D $^{1}$H–$^{13}$C PDLF NMR experiment in the whole mesophasic interval. The local orientational properties of the three rings of the aromatic core of **9HL** were determined in a robust way [86] in both the SmA and SmC* phases, and the temperature trend of the main orientational order parameters, $S_{zz}$, referring to the three rings is reported in Figure 8a.

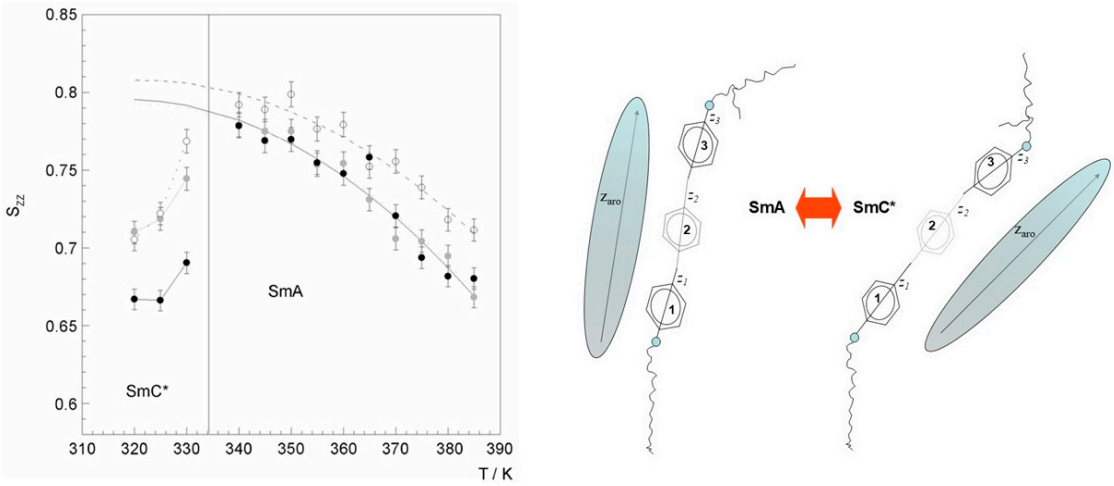


**Figure 8.** (**a**) Values of the order parameter $S_{zz}$ of the three aromatic rings of **9HL**: ring close to the achiral chain (grey circles), central ring (empty circles), and ring close to the lactate unit (black circles). Values were determined based on the analysis of the $^{1}$H-$^{13}$C PDLF NMR experiment. Solid and dashed curves are guidelines only. (**b**) Sketch of the two most probable conformations in the SmA and SmC* phases. Figures are reproduced and modified with permission from [86]. Copyright © 2014 John Wiley & Sons, Inc.

These trends are very interesting for gaining a better understanding of the conformational properties of the core of the LC mesogen in the SmA and in the SmC* phases. In fact, as it can be noticed in Figure 8a, the ring close to the chiral chain presents a higher tilt angle with respect to the other two rings, which are almost collinear, in the SmC* phase. On the contrary, in the SmA phase, the orientation of the three rings is very similar. A schematic representation of the relative orientation of the three rings of **9HL** in the two smectic phases is shown in Figure 8b. As reported for other ferroelectric liquid crystals [7,62,89], NMR investigations revealed a conformational change at the SmA–SmC* phase transition. In particular, the temperature trends of the measured $^{13}$C chemical shift of the alpha methylenoxy carbons (carbon-31 and carbon-34) in the chiral lateral chain at the SmA–SmC* transition supports the occurrence of a conformational change (see Figure 7b). The two carbon sites are characterized by an opposite trend of their chemical shift at the phase transition, thus indicating a different configuration of the lateral chain in the SmA and SmC* phases. This phenomenon has been observed in the other two smectogens, as shown in Section 3.3. The combination of $^{2}$H NMR and $^{13}$C NMR studies [84–86] gives additional clues concerning the correct models describing the 'de Vries' phases. All of these results are coherent with a more complex view of these LC systems; on one side, the occurrence of local clusters in the SmA phase and the presence of a significant tilt of the aromatic core are in agreement with the 'random diffuse core' model for the SmA phase formed by 'de Vries' LCs [29], and on the other side, the complete analysis of both $^{13}$C NMR chemical shift anisotropies and $^{1}$H–$^{13}$C PDLF NMR dipolar couplings is in agreement with a 'conformational change model' for the SmA–SmC* phase transition, as proposed in refs. [91,92].

3.2.2. Dynamic Properties of 'de Vries' LCs Obtained through NMR

The 'de Vries' liquid crystal **9HL** has been investigated by means of $^1$H NMR relaxometry to characterize the main dynamic processes active in a wide frequency range [93]. This technique is useful for measuring the $^1$H NMR relaxation times, $T_1$, as a function of the temperature and as a function of the proton Larmor frequency, $\nu_L$ [66]. In one study [93], measurements were carried out at $\nu_L$ = 100 MHz and in the interval between 18 MHz and 5 kHz by means of the Fast Field Cycling NMR technique. Examples of trends of measured relaxation rates (defined as the inverse of the relaxation time, $1/T_1$) in the temperature interval of existence of the SmA and SmC* phases of **9HL** are reported in Figure 9a–d. The differences among these four plots are related to the different motional processes active at different frequencies. For instance, at a high frequency (100 MHz), $T_1$ is sensitive to fast motions, such as the molecular reorientation motion (ROT). Moving to lower frequencies, additional processes need to be considered, such as the translational self-diffusion (SD) and the collective motions, namely, the layer undulations (LU), typical of smectic phases. The analysis of both the temperature dependence and the frequency dependence of $T_1$ for the **9HL** required the addition of a further motional process in the SmA close to the transition to the SmC* phase [93]. In fact, the frequency sweep curves recorded in the vicinity of the SmA–SmC* transition present an anomalous behavior with respect to typical SmA phases [66]. The proposed new mechanism is the in-layer tilting direction fluctuation (TDF), which is present in the SmC* phase due to the occurrence of tilted molecules with respect to the layer normal. As it can be seen in Figure 9a–d, the best fitting curves obtained with a global fitting procedure for all data sets reproduce very well the experimental data.

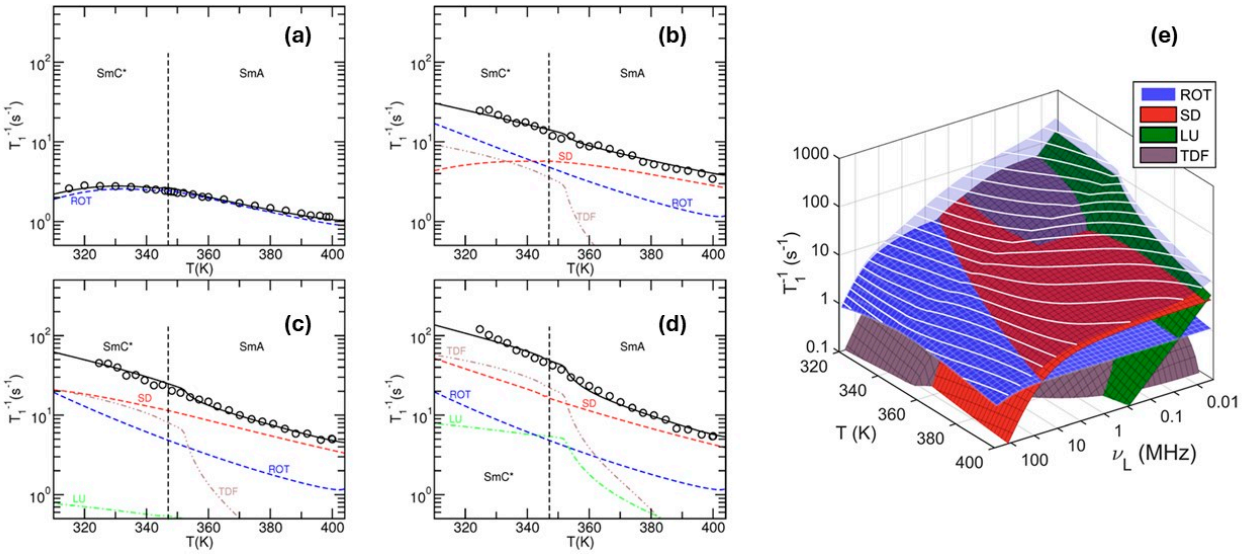


**Figure 9.** Experimental temperature-dependent relaxation rates, namely $1/T_1$ (s$^{-1}$), and model-fitting curves obtained for four values of the $^1$H Larmor frequencies: (**a**) $\nu_L$ = 100 MHz, (**b**) $\nu_L$ = 4 MHz, (**c**) $\nu_L$ = 1 MHz, and (**d**) $\nu_L$ = 100 kHz. (**e**) 3D plot showing the model fit surfaces obtained by using the best-fitting parameters of the experimental relaxation rates. White lines represent the lines of constant values of $1/T_1$, and the almost-transparent surface represents the sum of all contributions of $1/T_1$. ROT stands for 'rotational motion', SD stands for 'self-diffusion', LU stands for 'smectic layer undulations', and 'TDF' stands for in-layer tilting direction fluctuations. Reproduced with permission from [93]. Copyright © 2016 American Chemical Society.

The 3D plot shown in Figure 9e helps in better visualizing the relative contributions of the relaxation mechanisms to the $1/T_1$ dispersions and temperature dependencies [93] in the two mesophases. From the plot, it is possible to see the frequency and temperature regions where a dynamic mechanism is most prominent. For instance, in the high-frequency range (from 5 MHz to 100 MHz), the molecular reorientation motion (ROT) is the most

important dynamic process, in agreement with other studies based on the analysis of $^{2}$H NMR spin–lattice relaxation times both in the SmA and SmC* phases [94,95]. In the low-frequency range (from 100 kHz to 5 kHz), the smectic layer undulation (LU) is the most prominent dynamic mechanism in both smectic phases. However, in the intermediate-frequency range (from 5 MHz to 100 kHz), at high temperatures in the SmA, the main dynamic process is the translational self-diffusion (SD), while at low temperatures in the SmC*, the in-layer tilting direction fluctuation (TDF) is the most important process. Moreover, the discontinuities in the white lines, which correspond to lines of constant $1/T_1$ values, provide evidence for what happens from the dynamic point of view close to the SmA–SmC* phase transition. The occurrence of 'TDF' motions at intermediate frequencies already in the SmA phase is coherent with the formation of clusters of tilted LC molecules with the same azimuthal angle, thus confirming the validity of the proposed 'cluster cone model' to describe the molecular arrangement in the SmA formed by 'de Vries' LCs [93].

### *3.3. Conformational Properties of Calamitic Liquid Crystals in the SmC* Phase*

As reported in the previous section, the explanation of the transition between the SmA phase and the ferroelectric SmC* phase in terms of molecular properties has been object of several studies [7,62,84–86,89–92]. Most of them are in support of a significant change in the average conformation of the liquid crystal mesogen at the phase transition, which can in principle justify the appearance of a spontaneous polarization in the chiral smectic tilted phase [92]. Both theoretical [92] and experimental [86,89] studies provide evidence supporting the fact that the most probable conformer in the SmC* phases is bent with respect to the SmA phase, where the most probable conformer is the most alongated and thus uniaxial one. This hypothesis was supported by several NMR investigations, including one concerning the 'de Vries' liquid crystal **9HL** described in the previous section. An example of a detailed study of the conformational properties of a ferroelectric smectogen, namely the **M10/****, was reported in 2010 [96]. This case is interesting, since the LC smectogen does not present a SmA phase. At high temperatures, this compound shows the optically isotropic Blue phase (BPII) and the cholesteric phase (N*), followed at lower temperatures by an SmC* phase stable in a wide temperature range [96]. The work presents a detailed conformational study based on the analysis of experimental $^{13}$C NMR data in combination with the DFT approach mostly focused on the two lateral chains, the chiral chain containing two chiral carbon centers and the achiral chain of the **M10/**** sample (see the molecular structure in Figure 10a). The $^{13}$C CP NMR spectra recorded in the mesophases are reported in Figure 10a. Both the BPII and N* phases are characterized by relatively broad and not-well-resolved peaks, and this can be easily explained by the isotropic nature of the BPII phase and the presence of a distribution of orientations of the phase directors in the N* phase. When the SmC* phase occurs, the $^{13}$C CP NMR peaks become more defined, and a significant change in the chemical shift of most of the carbon signals is observed. The trend of the observed chemical shift as a function of temperature in the SmC* phase is the opposite of that reported in Figure 7d for the **9HL** sample. In fact, the observed $^{13}$C chemical shifts of the aromatic carbons (from 125 to 250 ppm) increase markedly at the phase transition between the N* and SmC* phases, and at lower temperatures, they continue increasing by decreasing the temperature. On the contrary, those of the aliphatic carbons (from 0 to 50 ppm) decrease slightly [96].

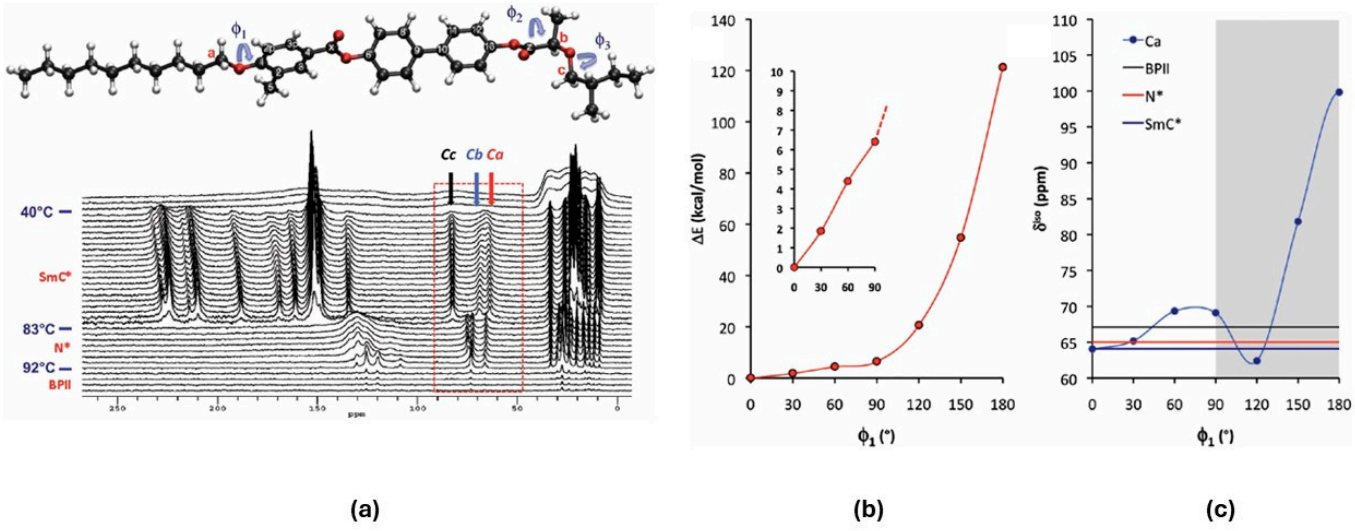


**Figure 10.** (**a**) (top) Molecular structure of the **M10/**** sample. Relevant carbons and dihedral angles are marked. (Bottom) $^{13}$C NMR spectra of **M10/**** as a function of the temperature in the three mesophases: BPII, N*, and SmC*. The dashed red box shows the alkoxylic $^{13}$C signals (relative to carbons Ca, Cb, and Cc). (**b**) The conformational energy, ΔE (kcal/mol), as a function of the dihedral angle $\varphi_1$ (°) in the 0–180° range. An expansion of the plot, in the range of 0–90°, is shown in the inset. (**c**) The calculated isotropic $^{13}$C chemical shift, $\delta_{iso}$, for the Ca carbon on the achiral chain as a function of $\varphi_1$. The experimental values of the $^{13}$C chemical shift observed in the BPII, N*, and SmC* phases are also displayed (continuous lines). The grey area represents the region corresponding to energy greater than 6 kcal/mol, which means 0% population according to Boltzmann distribution analyses performed in the 25–125 °C temperature range. Reprinted with permission from [96]. Copyright © 2010 American Chemical Society.

This behavior is due to the total unwinding of the helical structure in the SmC* phase of the **M10/**** sample, thus indicating that for this mesogen, the operating NMR magnetic field of 9.4 T is higher than the critical field. The research is focused on the interpretation of the trend of the signals in the region from 50 to 100 ppm, which corresponds to the signals of the alkoxylic carbons Ca, Cb, and Cc (see Figure 10a). With respect to other $^{13}$C signals, the observed chemical shift of these carbons changes abruptly at each phase transition, while it remains almost constant within each mesophase. To understand these trends of the $^{13}$C NMR chemical shift, detailed DFT calculations of the potential energy surfaces and of the $^{13}$C NMR isotropic chemical shifts have been performed [96]. In particular, a conformational study was performed, and the chemical shift tensors of the three carbons (Ca, Cb, and Cc) were determined through DFT calculations. The most populated conformers of the **M10/**** compound in the three phases were identified by comparing the observed chemical shift with the computed chemical shift. In this step, an approximation was introduced; we have assumed that the chemical shift anisotropies are negligible, thus identifying the observed chemical shift measured in the static $^{1}$H decoupled $^{13}$C CP NMR spectra with the theoretical isotropic chemical shift ($\delta = \delta_{iso}$). For the three mesophases, a unique set of the dihedral angles $\varphi_1$, $\varphi_2$, and $\varphi_3$ (defined in Figure 10a) was identified, and an average conformation of the **M10/**** compound was determined. For simplicity, the conformational energy, ΔE (kcal/mol), as a function of the dihedral angle $\varphi_1$ relative to the carbon Ca is reported in Figure 10b. The plot clearly shows that the most stable conformation for Ca is obtained for $\varphi_1 = 0°$; in fact, ΔE increases with the increase in the dihedral angle from 0° to 180°. The conformations with $\varphi_1 > 90°$ have very high energy. Interestingly, DFT calculations indicate that the chemical shift of the carbon on the achiral chain (Ca) is very sensitive to the dihedral angle $\varphi_1$. As seen in Figure 10c, the region marked in grey indicates that the values of the dihedral angle between 90° and 180° can be excluded, as they correspond to high energy (6 kcal/mol < E < 120 kcal/mol). By considering the

temperature range of stability of the three mesophases, from 25° to 125 °C, these values of the dihedral angle correspond to about 0% population and very distorted molecular geometries. Similar procedures were performed for the dihedral angles $\varphi_2$ and $\varphi_3$. In these cases, two intervals, namely, 120–180° for $\varphi_2$ and 150–180° for $\varphi_3$, can be excluded as they correspond to high energy and a low population. In Figure 10c, the calculated values of the chemical shift, $\delta_{iso}$, are superimposed onto the three values of the observed chemical shift, $\delta$, in the three mesophases. The intersection between the calculated and experimental curves allowed us to identify the average conformation in the three phases [96]. In conclusion, the study demonstrated that the **M10/**** sample undergoes to a conformational change concerning the lateral aliphatic moieties at the two phase transitions. In particular, the achiral chain reduces its degrees of freedom by decreasing the temperature, while the chiral chain assumes different stable conformations and, as a consequence, the overall molecular shape of the **M10/**** is different in the three different mesophases. Moreover, from the analysis of the $^{13}C$ NMR chemical shift anisotropy in the ferroelectric SmC* phase, the local orientational orders, $S_{zz}$ and $S_{xx}$-$S_{yy}$, could be determined, showing a molecular biaxiality that was rather large, which is in agreement with other studies on several ferroelectric LCs [48,88]. The present investigations confirm that in the SmC* phase, the overall molecular shape is bent and not linear as in highly ordered mesophases. As a main result, the study supports the hypothesis of a conformational change of the mesogens at the origin of the properties of the ferroelectric SmC* phase.

## 4. The Ferroelectric and Antiferroelectric Smectic Phases

Among chiral smectogens, several series of rod-like compounds possess the SmC* and the $SmC^*_A$ phases, with the typical synclinic and anticlinic structures, such as those represented in Schemes 1 and 2. Several studies are reported in the literature about NMR investigations of the ferroelectric and antiferroelectric smectic phases [60,64,71,90,94,97–103]. In the following paragraphs, some of the main results obtained by means of different NMR techniques are reported.

### *4.1. Ordering Properties and Tilt Angle in the Ferroelectric and Antiferroelectric Smectic Phases of Calamitic Liquid Crystals*

A smectogen that was intensively investigated through several NMR techniques is the **ZLL 7/*** [60,64,76,94], whose molecular structure is reported in Figure 11a. This compound, which has three chiral carbon centers, shows the following mesophases: SmA, SmC*, $SmC^*_A$, re-entrant SmC* ($SmC^*_r$), and hexatic (Hex). The trend of the spontaneous polarization and the optical tilt angle in the tilted mesophases does not show any discontinuity at the transitions SmC*–$SmC^*_A$ or $SmC^*_A$–$SmC^*_r$ (see Figure 11b) [60]. In particular, the trend of the optical tilt angle increases rapidly in the SmC* phase, and then it continues to increase slowly by decreasing the temperature in both $SmC^*_A$ and $SmC^*_r$, while it starts decreasing in the hexatic phase until the crystalline phase appears. As shown in Figure 11b, there are some differences among the deuterated isotropomers and the not-deuterated one, and this has also been observed for other deuterated and not-deuterated compounds [48,51,60]. The study performed by means of $^2H$ NMR spectroscopy on two isotopomers selectively deuterated on the phenyl and biphenyl fragments gave some additional information that was useful for better identifying the mesophase transition and for obtaining both ordering and conformational properties. As for the previous section, the experimental details of the NMR investigations are not reported here, as they have been published in ref. [60].

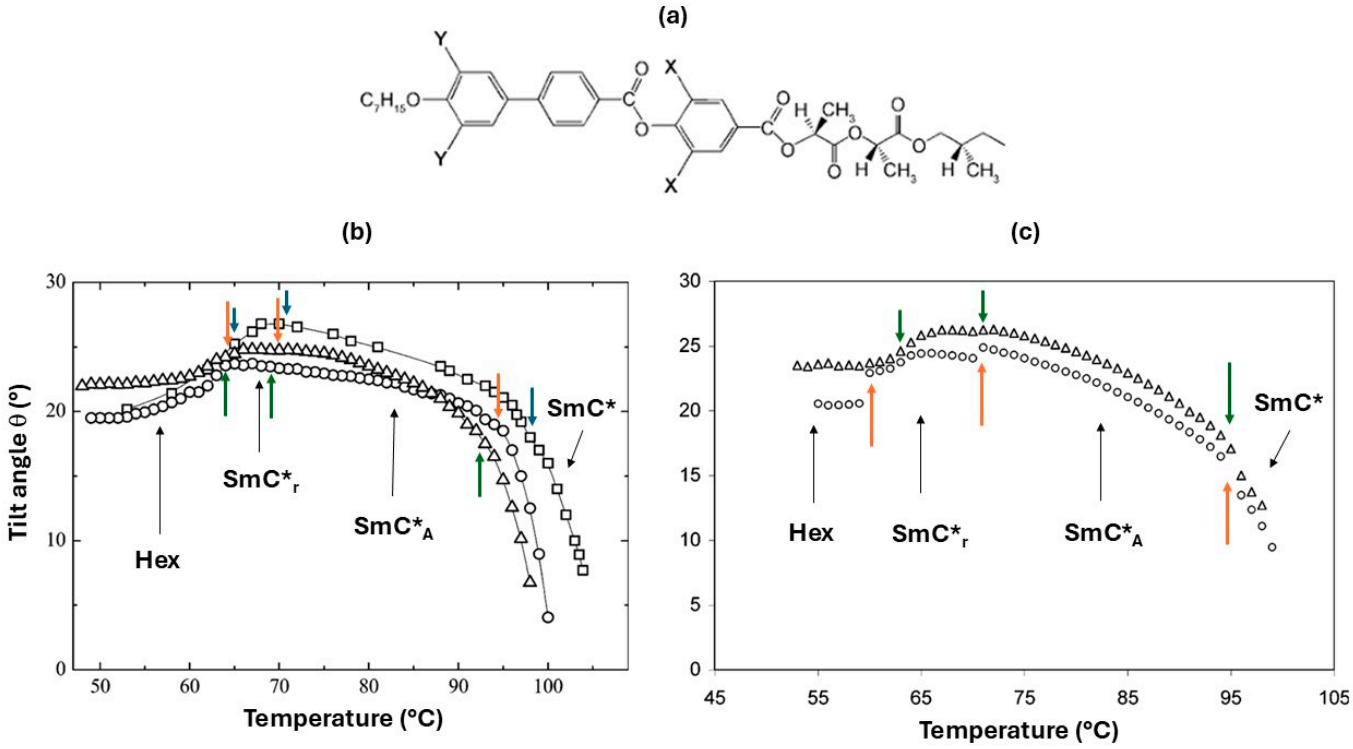


**Figure 11.** (**a**) Molecular structure of the ZLL7/* (X = Y = H) and the two isotopomers **ZLL7/*-phe-d$_2$** (X = D, Y = H) and **ZLL7/*-biphe-d$_2$** (X = H, Y = D). (**b**) Temperature dependence of the spontaneous tilt angle measured optically upon cooling for **ZLL 7/*** (empty squares), **ZLL 7/*-phe-d$_2$** (empty circles), and **ZLL 7/*-biphe-d$_2$** (empty triangles). (**c**) Tilt angle of the two labeled **ZLL 7/*** compounds vs. temperature based on the $^2$H NMR study. Triangles and circles refer to **ZLL 7/*-biphe-d$_2$** and **ZLL 7/*-phe-d$_2$**, respectively. The experimental error is lower than 3%. Vertical colored arrows indicate the temperature transitions for **ZLL 7/*** (blue arrows), **ZLL 7/*-phe-d$_2$** (orange arrows), and **ZLL 7/*-biphe-d$_2$** (green arrows). Adapted with permission from [60]. Copyright © 2006 American Chemical Society.

The values of the of tilt angle, $\theta$, obtained from the analysis of $^2$H NMR quadrupolar splittings for the two deuterated samples, are reported in Figure 11c in the temperature range of stability of the mesophases. The tilt angles are slightly higher for **ZLL 7/*-biphe-d$_2$** than for **ZLL 7/*-phe-d$_2$**. As it can be seen, the transition SmC*–SmC*$_A$ is characterized by a sudden increase in the tilt angle, while the transition SmC*$_A$–SmC*$_r$ is characterized by an opposite but smaller jump. Moreover, the tilt angle is reduced in the hexatic phase, similarly to what observed for the optical tilt angle [60]. Both techniques indicate that the larger tilt angle is observed in the SmC*$_A$ phase in the vicinity or in correspondence with the SmC*$_r$ phase, and the higher value is about 26.5°. By comparing the trend of the optical tilt angle with those of the NMR tilt angle and with the trend of the layer spacing obtained through X-ray, the discontinuity observed in the tilt angle at the SmC*–SmC*$_A$ phase transition determined through $^2$H NMR (Figure 11c) suggests that an effective elongation of the molecule due to a conformational change could explain this discontinuity [60]. A peculiarity of this compound is the appearance of a rehentrant ferroelectric phase (SmC*$_r$). Recently, a paper has been published proposing a theoretical model explaining the mesophase behavior of the series of compound ZLL *m*/* based on a molecular statistical approach [104].

The analysis of $^2$H NMR spectra for the two isotopomers allowed us to determine the orientational order of the two deuterated fragments in the whole mesophasic range. Between the two deuterated moieties, the one with the higher orientational order is the biphenyl fragment in almost all mesophases. For this moiety, $S_{zz}$ reaches a very high value (~1) at low temperatures in the hexatic phase. This means that the para axis of the biphenyl moiety can be considered almost coincidental with the long molecular axis and

with the phase director. Moreover, the fragment biaxiality could also be determined from the analysis of $^{2}$H NMR spectra, indicating that the biphenyl moiety of the **ZLL 7/*** sample can be safely assumed to be uniaxial in all smectic phases, while the phenyl ring, which is close to the achiral chain, is biaxial, with values of fragment biaxiality, defined as $S_{yy}$-$S_{xx}$, in the range of 0.04–0.06. These results were confirmed by $^{13}$C NMR experiments on the **ZLL 7/*** sample [64]. The hypothesis of a conformational change at the SmC*–SmC*$_A$ phase transition, in particular from a bent to a more elongated conformer, has been proposed for other LC compounds with ferroelectric and antiferroelectric phases based on $^{19}$F NMR [103] and $^{13}$C NMR [100].

### *4.2. Dynamic Properties in the Ferroelectric and Antiferroelectric Smectic Phases of Calamitic Liquid Crystals*

Several NMR studies have also been performed to study the behavior at the SmC*–SmC*$_A$ phase transition from a dynamic point of view.

$^{2}$H NMR relaxation times, both spin–spin and spin–lattice ones, have been measured and analyzed for the smectogen **ZLL 7/*** [94]. The trends of the spin–lattice relaxation times, $T_{1Z}$ and $T_{1Q}$, are reported in Figure 12a,b for the two isotopomers, **ZLL 7/*-biphe-d$_2$** and **ZLL 7/*-phe-d$_2$**, respectively. These trends present a quite complex dynamic behavior, which can be commented on by considering the presence of three different motional regimes: narrowing regime (fast motions), intermediate regime (intermediate motions), and slow regime (slow motions). The first regime is typical of the SmA and SmC* phases of calamitic liquid crystals, as reported in Section 2.2 and observed in several LC compounds [47–49]; the relaxation times, $T_{1Z}$ and $T_{1Q}$, decrease by decreasing the temperature, and this is an indication of a narrowing regime of motions. A second motional regime, characterized by a minimum in the trend of relaxation times, is observed in the SmC*$_A$ and SmC*$_r$ phases. Here, the main dynamic processes responsible for the longitudinal relaxation times are in the intermediate regime. In this case, it is possible to estimate the characteristic correlation times of the motions, namely $\tau_c$ equal to $2.2 \times 10^{-8}$ s and $1.6 \times 10^{-8}$ s, at the Larmor frequencies of the NMR spectrometers, 46.04 MHz and 61.38 MHz, respectively. A third motional regime is observed in the hexatic phase. Here, the relaxation times increase by decreasing the temperature, and this is an indication that the motions responsible for the longitudinal relaxation times are in the slow regime [94]. The quantitative analysis of these relaxation times in terms of theoretical models describing the main dynamic processes has been performed in the SmA and in the SmC* phase, as the limit of application of such models is the narrowing regime of motions. As a main result, the reorientational motions that typically affect the spin–lattice relaxation times in the fast regime of motions do not show significant changes in the activation energy in the two mesophases; however, the tumbling motion ($D_\perp$) and the reorientation around the para axis of the phenyl fragment ($D_{R\,(Phe)}$) are about one order of magnitude and a half smaller in the SmC* phase than in the SmA phase [94], thus indicating some restrictions due to the particular supramolecular structure of the ferroelectric phase. The occurrence of a minimum of the trend of $T_{1Z}$ and $T_{1Q}$ in the antiferroelectric phase can be interpreted qualitatively as a further restriction and, consequently, a slowing down of the reorientations in the anticlinic phase.

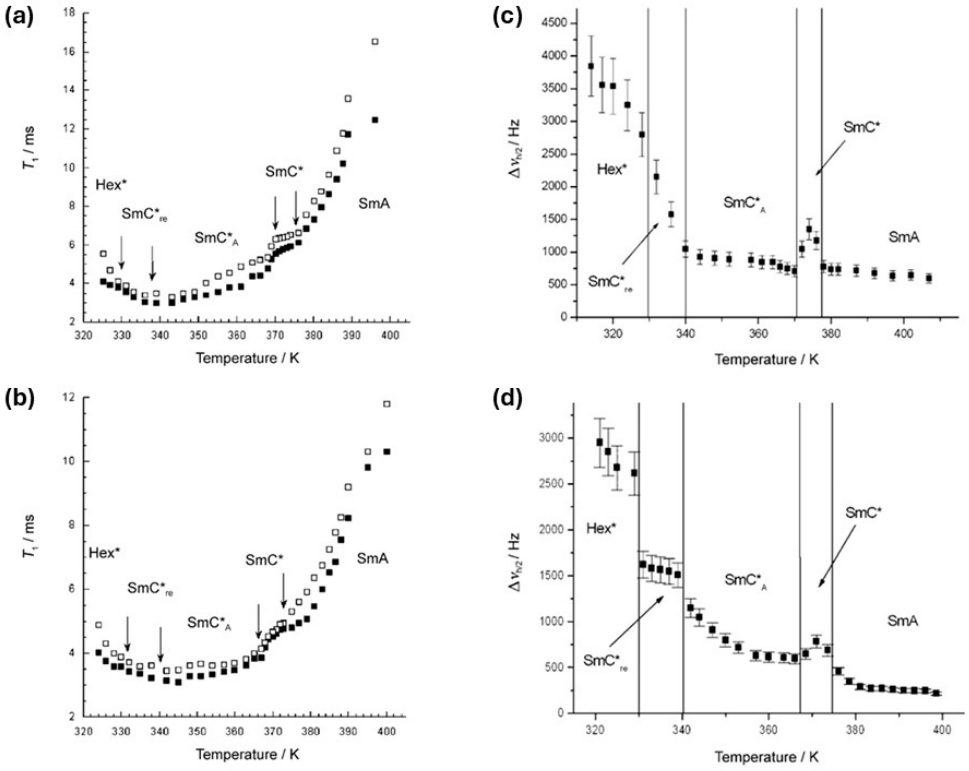


**Figure 12.** On the left, $^2$H NMR relaxation times (ms) $T_{1Q}$ (full squeres) and $T_{1Z}$ (empty squares) vs. temperature (K) measured at 46.04 MHz (magnetic field of 7.05 T) in the whole mesomorphic range of the isotopomers. (**a**) **ZLL7/*-biphe-d$_2$** and (**b**) **ZLL7/*-phe d$_2$**. On the right, experimental $^2$H NMR linewidth, $\Delta\nu_{h/2}$ (Hz) vs. temperature (K), determined at 46.04 MHz, in the whole mesomorphic range of the (**c**) **ZLL7/*-biphe-d$_2$** isotopomer and (**d**) **ZLL7/*-phe-d$_2$** isotopomer. Reproduced with permission from [81]. Copyright © 2009 John Wiley & Sons, Inc.

Further information concerning the dynamic processes active in the different mesophases can be obtained from the trends of the experimental $^2$H NMR spectral linewidths, $\Delta\nu_{h/2}$, as well as from those of the spin–spin relaxation times, $T_2$ [94]. Figure 12 shows the spectral linewidths obtained from the $^2$H NMR spectra recorded at 46.04 MHz for **ZLL7/*-biphe-d$_2$** (Figure 12c) and **ZLL7/*-phe-d$_2$** (Figure 12d).

From these trends, several considerations emerge, as follows: (i) the spectral linewidth increases by decreasing the temperature for both samples; (ii) in both cases, a jump is observed in the ferroelectric phase, thus indicating a sudden increase in the linewidth, which has been observed also in other ferroelectrics [50,105], interpreted either in terms of slower dynamics or static heterogeneities; and (iii) the two fragments have different behaviors at the SmC*$_A$–SmC*$_r$ and SmC*$_r$–Hex phase transitions. In particular, from the analysis of both spectral linewidth and spin–spin relaxation times, it is evident that there is a higher sensitivity of the phenyl ring closer to the chiral chain and to the phase transitions. The comparison between the spin–spin relaxation times, $T_2$*, obtained from the linewidth and one of the measured $T_2$ components [94] indicates that motions affecting the phenyl moiety are slower in the middle of the SmC*$_A$ phase, and they continue in this regime in the SmC*$_r$ phase, while in the case of the biphenyl fragment, the slowing down of the dynamic processes occurs in the sole SmC*$_r$ phase. A possible explanation is that in the SmC* and SmC*$_A$ phases the phenyl moiety is more influenced by slower motions, such as the layer undulations, while the most oriented biphenyl moiety is more influenced by the overall rotational diffusion motions. The smaller component of the measured relaxation times, $T_2$ [94], is probably influenced by slow reorientations, which can be associated with Goldstone and soft modes, as detected through dielectric measurements [106]. In fact, the Goldstone modes in the ferroelectric phase have a typical frequency of a few

hundred hertz, thus representing one of the main contributions to the high permittivity of the ZLL 7/* sample in the synclinic supramolecular arrangement. On the contrary, in the antiferroelectric phase, Goldstone modes are smaller, while the soft modes with a frequency of tens of kilohertz are more important.

The same compound has been investigated by means of $^1$H NMR diffusometry [71]. The self-diffusion coefficients measured in the isotropic phase ($D_{sd}$) and for two orthogonal directions ($D_{sd}$ (//) and $D_{sd}$ (⊥)) in the SmA, SmC*, and SmC*$_A$ phases are reported in Figure 13.

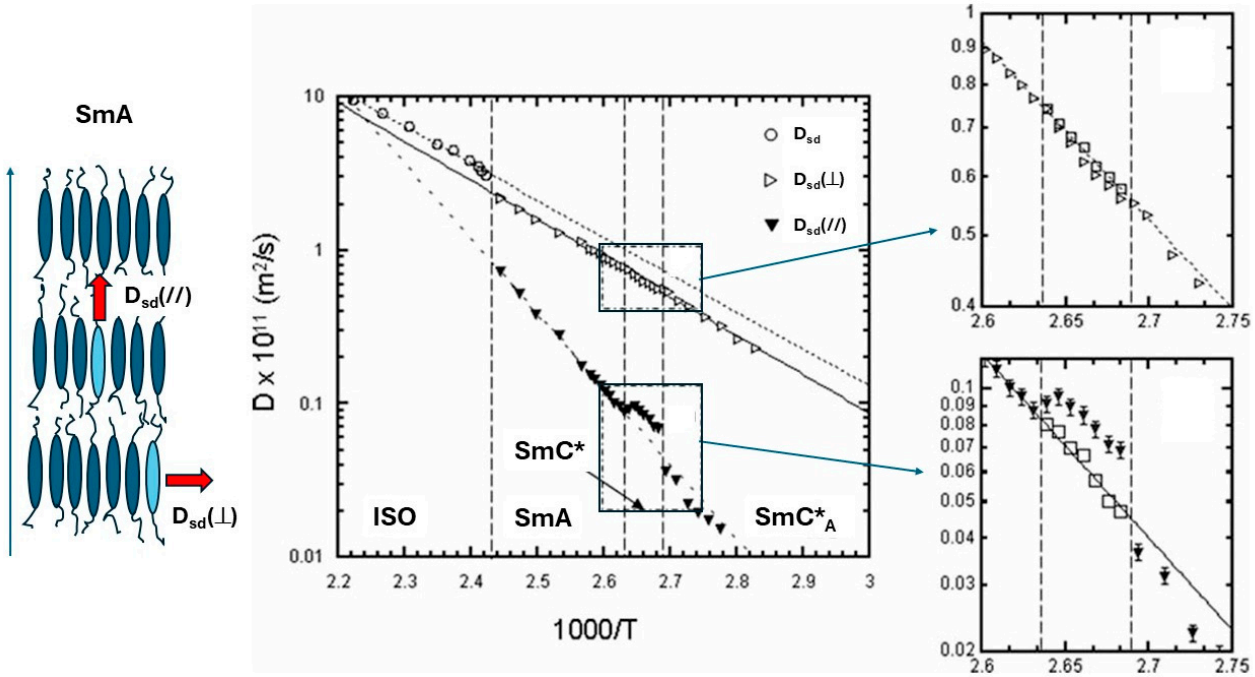


**Figure 13.** Self-diffusion coefficients ($D_{sd}$) of **ZLL 7/*** measured through $^1$H NMR PFG diffusometry in the isotropic and liquid crystalline phases. On the right, two inserts show the expanded views at the transitions SmA–SmC*–SmC*$_A$ for diffusion measured along the mesophase layer normal (//) and perpendicular to it (⊥), respectively. In the inserts, open squares indicate intra- and inter-layer diffusion coefficients in the ferroelectric phase, calculated as discussed in ref. [71]. Where not explicitly reported, error bars are smaller than the relative symbols. Adapted with permission from [71]. Copyright © 2010 Royal Society of Chemistry.

As shown in Figure 13, in the isotropic phase a single value of diffusion constant ($D_{sd}$) is measured. When approaching to the smectic A phase, the diffusion constant rapidly decreases and two different values of diffusion coefficient can be measured: the diffusion along the normal of smectic layer ($D_{sd}$//), corresponding to inter layer molecular translation, and the diffusion in the smectic layer which is the intra-layer diffusion ($D_{sd}$⊥). Typically, $D_{sd}$// is smaller than $D_{sd}$⊥, as reported in Figure 13. Interestingly, when entering the ferroelectric phase, small discontinuities can be observed in both diffusion coefficients. In particular, $D_{sd}$// is much more affected by the occurrence of the tilted synclinic phase than $D_{sd}$⊥. A small discontinuity is also observed at the SmC*-SmC*$_A$ phase transition. From the trend of the diffusion coefficients as a function of temperature, and by assuming an Arrhenius law, the activation energies are 95 kJ/mol and 47 kJ/mol for inter- and intra-layer diffusion processes, respectively. The small discontinuities observed in this work are in agreement with the role of the layered structure of the smectic phases in determining the main anisotropic character of the diffusion. The diffusion discontinuities associated with the different arrangement of molecules from the synclinic to the anticlinic phase could be a validation test for the theoretical models concerning the ferroelectric and antiferroelectric phase transition. A change in the dynamic properties at the ferroelectric-antiferroelectric

phase transition is in agreement with previous observations on different smectogens, based on $^{2}$H NMR [97–99] and $^{13}$C NMR relaxation studies [100,101].

## 5. Conclusions and Future Perspectives

This review reports several studies conducted on chiral smectic calamitic liquid crystals forming the SmA, SmC*, and SmC*$_A$ based on NMR spectroscopy. Local ordering properties, such as order parameters referring to different fragments of the smectogens, were investigated by means of $^{2}$H NMR spectroscopy in several LC compounds with two aromatic moieties, the biphenyl and the phenyl ones, typically connected by an ester group. Most of these studies showed that the fragment closer to the achiral chain is the most oriented in the SmA and in the other smectic phases; however, the angle between the para axes of these fragments changes upon passing from one smectic phase to another, thus indicating that the average conformer is different in each mesophase. $^{2}$H NMR spectroscopy was a fundamental technique to understand the effect of an external magnetic field applied parallel to the helical axis of the ferroelectric smectic, SmC*, phase, and it stimulated the development of a phenomenological model to explain the occurrence of the critical magnetic field for the unwinding of the helical supramolecular structure in terms of molecular properties of the LC compounds. $^{2}$H NMR combined with $^{13}$C NMR spectroscopy was indeed very useful in clarifying the conformational properties of these smectogens in the SmA, SmC*, and SmC*$_A$ phases. A detailed study was reported here concerning a 'de Vries' liquid crystal with three rings in the aromatic core. This investigation allowed for the determination of the temperature dependence of the local orientational order parameter, $S_{zz}$, for the three rings, clearly indicating a conformational change at the SmA–SmC* phase transition. Moreover, the complete study based on complementary NMR techniques, such as $^{2}$H NMR, $^{13}$C CP NMR, and $^{1}$H-$^{13}$C PDLF scaled dipolar coupling NMR experiments on the same smectogen, supported the explanation of the 'de Vries' features in terms of 'random diffuse cone' and 'conformational change' models. Several NMR techniques, such as the experiments to obtain $^{2}$H NMR relaxation times, $^{1}$H NMR relaxometry, and $^{1}$H NMR diffusometry, were also applied to chiral smectic phases. This review aims to show some significant studies based on the analysis of relaxation times in terms of dynamic models, which were useful for the complete characterization of the main motional processes and dynamic mechanisms in the SmA and in the ferroelectric SmC* phase. A particular case concerning a smectogen showing ferroelectric and antiferroelectric phases is reported based on $^{1}$H NMR diffusometry, which supports the hypothesis of a significant change in dynamics at the SmC*–SmC*$_A$ phase transition. The cases described in this review are interesting and could be inspiration for future NMR studies to understand conformational, orientational, and dynamic properties of new mesophases, such as the nematic ferroelectrics, the highly tilted smectic phases, such as the orthoconic antiferroelectrics, and other highly polar smectic phases.

**Funding:** This research received no external funding.

**Conflicts of Interest:** The author declares no conflicts of interest.

## References

1. Meyer, R.B.; Liebert, L.; Strzelecki, L.; Keller, P. Ferroelectric liquid crystals. *J. Phys. Lett.* **1975**, *36*, L69–L71. [CrossRef]
2. Meyer, R.B. Ferroelectric liquid crystals; a review. *Mol. Cryst. Liq. Cryst.* **1977**, *40*, 33–48. [CrossRef]
3. Goodby, J.W.; Blinc, R.; Clark, N.A.; Lagerwall, S.T.; Osipov, A.; Pikin, S.A.; Sakurai, T.; Yoshino, K.; Zeks, B. *Ferroelectric Liquid Crystals, Principles, Properties and Applications*, 1st ed.; Gordon and Breach: Philadelphia, PA, USA, 1991.
4. Goodby, J.W. Twisted and frustrated states of matter. *Proc. R. Soc. A* **2012**, *468*, 1521–1542. [CrossRef]
5. Dierking, I. Chiral Liquid Crystals: Structures, Phases, Effects. *Symmetry* **2014**, *6*, 444–472. [CrossRef]
6. Guo, Q.; Yan, K.; Chigrinov, V.; Zhao, H.; Tribelsky, M. Ferroelectric liquid crystals: Physics and applications. *Crystals* **2019**, *9*, 470. [CrossRef]
7. Yoshizawa, A. Ferroelectric Smectic Liquid Crystals. *Crystals* **2024**, *14*, 350. [CrossRef]
8. Clark, N.A.; Largerwall, S.T. Submicrosecond bistable electro-optic switching in liquid crystals. *Appl. Phys. Lett.* **1980**, *36*, 899–901. [CrossRef]

9. Walba, D.M. Fast ferroelectric liquid-crystal electro-optics. *Science* **1995**, *270*, 250. [CrossRef]
10. Chandani, A.D.L.; Gorecka, E.; Ouchi, Y.; Takezoe, H.; Fukuda, A. Antiferroelectric chiral smectic phases responsible for the tristable switching in MHPOBC. *Jpn. J. Appl. Phys.* **1989**, *28*, L1265–L1268. [CrossRef]
11. Nishiyama, I. Antiferroelectric liquid crystals. *Adv. Mater.* **1993**, *6*, 966–970. [CrossRef]
12. Fukuda, A.; Takanishi, Y.; Isozaki, T.; Ishikawa, K.; Takezoe, H. Antiferroelectric chiral smectic liquid crystals. *J. Mater. Chem.* **1994**, *4*, 997–1016. [CrossRef]
13. Lagerwall, S.T. Orthoconic liquid crystals—A case study. *Adv. Colloid Interface Sci.* **2014**, *208*, 1–9. [CrossRef] [PubMed]
14. Urbanska, M.; Dardas, D. Properties of Antiferroelectric Mixtures Differing in the Amount of Added Racemate. *Crystals* **2024**, *14*, 147. [CrossRef]
15. Hobbs, J.; Gibb, J.C.; Mandle, R.J. Emergent Antiferroelectric Ordering and the Coupling of Liquid Crystalline and Polar Order. *Small Sci.* **2024**, 2400189. [CrossRef]
16. Pandey, M.B.; Dabrowski, R.; Dhar, R. *Antiferroelectric Liquid Crystals: Smart Materials for Future Displays in Advanced Energy Materials*; Tiwari, A., Valyukh, S., Eds.; WILEY-Scrivener Publishing: Beverly, MA, USA, 2014; pp. 389–432. [CrossRef]
17. Rudquist, P. Orthoconic antiferroelectric liquid crystals. *Liq. Cryst.* **2013**, *40*, 1678. [CrossRef]
18. Zurowska, M.; Dziaduszek, J.; Szala, M.; Morawiak, P.; Bubnov, A. Effect of lateral fluorine substitution far from the chiral center on mesomorphic behaviour of highly titled antiferroelectric (S), and (R) enantiomers. *J. Mol. Liq.* **2018**, *267*, 504–510. [CrossRef]
19. Dąbrowski, R.; Kula, P.; Raszewski, Z.; Piecek, W.; Oton, J.M.; Spadło, A. New orthoconic antiferroelectrics useful for applications. *Ferroelectrics* **2010**, *395*, 116–132. [CrossRef]
20. Gupta, D.; Kula, P.; Bhattacharjee, A. Mesomorphic, electro-optic and dielectric behaviour of a semi-fluorinated chiral liquid crystalline material forming polar smectic phases. *J. Mol. Struc.* **2020**, *1219*, 128557. [CrossRef]
21. Gupta, D.; Kula, P.; Bhattacharjee, A. Investigation of a partially fluorinated chiral antiferroelectric liquid crystalline material with large negative dielectric anisotropy. *J. Mol. Struc.* **2021**, *331*, 115704. [CrossRef]
22. Urbanska, M.; Gratzke, M.; Czerwinski, M.F. Synthesis and Characterization of New Chiral Smectic Four-Ring Esters. *Molecules* **2024**, *13*, 3134. [CrossRef]
23. Tykarska, M.; Kurp, K.; Mironov, S.; Rychlowicz, N.; Karcz, J.; Dziaduszek, J.; Kula, P.; Stulov, S.; Bubnov, A. Tuning of self-organizing and electro-optical behaviour for orthoconic ferroelectric liquid crystal by non-chiral dopants. *J. Mol. Liq.* **2024**, *409*, 125426. [CrossRef]
24. Dwivedi, A.; Dwivedi, S.; Pandey, M.B.; Dabrowski, R.; Dhar, R. Collective molecular relaxations and electro-optical switching response of a wide room temperature antiferroelectric liquid crystal mixture. *Opt. Mater.* **2024**, *149*, 115016. [CrossRef]
25. Nepal, S.; Das, B.; Das, M.K.; Das Sarkar, M.; Strójwas, K.; Dmochowska, E.; Czerwinski, M. High tilted antiferroelectric liquid crystals: Polymer-based approach for phase stabilisation and device development. *J. Mol. Liq.* **2023**, *375*, 121297. [CrossRef]
26. Strójwjs, K.; Dabrowski, R.; Drzewinski, W.; Szarek, M.; Bubnov, A.; Czerwinski, M. The comparison of self-assembling behaviour of phenyl biphenylcarboxylate and biphenyl benzoate compounds with the different length and shape of chiral terminal chain. *J. Mol. Liq.* **2023**, *369*, 120882. [CrossRef]
27. Clark, N.A.; Rieker, T.P. Smectic-C "chevron", a planar liquid-crystal defect: Implications for the surface-stabilized ferroelectric liquid-crystal geometry. *Phys. Rev. A* **1988**, *37*, 1053–1056. [CrossRef]
28. de Vries, A. X-ray photographic studies of liquid crystals: II. Apparent molecular length and thickness in three phases of ethyl-p-ethoxybenzal-p-aminobenzoate. *Mol. Cryst. Liq. Cryst.* **1970**, *11*, 361–383. [CrossRef]
29. de Vries, A. Experimental evidence concerning two different kinds of smectic C to smectic A transitions. *Mol. Cryst. Liq. Cryst.* **1977**, *41*, 27–31. [CrossRef]
30. Lagerwall, J.P.F.; Giesselmann, F. Current Topics in Smectic Liquid Crystal Research. *ChemPhysChem* **2006**, *7*, 20–45. [CrossRef]
31. Diele, S.; Brand, P.; Sackmann, H. X-ray Diffraction and Polymorphism of Smectic Liquid Crystals 1. A-, B- and C-modifications. *Mol. Cryst. Liq. Cryst.* **1972**, *16*, 105. [CrossRef]
32. Niori, T.; Sekine, F.; Watanabe, J.; Furukawa, T.; Takezoe, H. Distinct ferroelectric smectic liquid crystals consisting of banana shaped achiral molecules. *J. Mater. Chem.* **1996**, *6*, 1231. [CrossRef]
33. Sekine, T.; Niori, T.; Sone, M.; Watanabe, J.; Choi, S.-W.; Takanishi, Y.; Takezoe, H. Origin of helix in achiral banana-shaped molecular systems. *Jpn. J. Appl. Phys.* **1997**, *36*, 6455–6463. [CrossRef]
34. Reddy, R.A.; Zhu, C.; Shao, R.; Korblova, E.; Gong, T.; Shen, Y.; Garcia, E.; Glaser, M.A.; Maclennan, J.E.; Walba, D.M.; et al. Spontaneous ferroelectric order in a bent-core smectic liquid crystal of fluid orthorhombic layers. *Science* **2011**, *332*, 72–77. [CrossRef]
35. Tschierske, C.; Ungar, G. Mirror symmetry breaking by chirality synchronization in liquids and liquid crystals of achiral molecules. *ChemPhysChem* **2016**, *17*, 9–26. [CrossRef] [PubMed]
36. Song, Y.; Aya, S.; Huang, M. Updated view of new liquid-matter ferroelectrics with nematic and smectic orders. *Giant* **2024**, *19*, 100318. [CrossRef]
37. Mandle, R.J.; Cowling, S.J.; Goodby, J.W. A nematic to nematic transformation exhibited by a rod-like liquid crystal. *Phys. Chem. Chem. Phys.* **2017**, *19*, 11429–11435. [CrossRef]
38. Mandle, R.J.; Cowling, S.J.; Goodby, J.W. Rational design of rod-like liquid crystals exhibiting two nematic phases. *Chem. A Eur. J.* **2017**, *23*, 14554–14562. [CrossRef]

39. Nishikawa, H.; Shiroshita, K.; Higuchi, H.; Okumura, Y.; Haseba, Y.; Yamamoto, S.; Sago, K.; Kikuchi, H. A fluid liquid-crystal material with highly polar order. *Adv. Mater.* **2017**, *29*, 1702354. [CrossRef]
40. Lavrentovich, O.D. Ferroelectric nematic liquid crystal, a century in waiting. *Proc. Natl. Acad. Sci. USA* **2020**, *117*, 14629–14631. [CrossRef]
41. Sreenilayam, S.P.; Brabazon, D.; Panarin, Y.P. Fast Ferroelectric Liquid Crystal Based Optical Switch: Simulation and Experiments. *Crystals* **2019**, *9*, 388. [CrossRef]
42. Pozhidaev, E.P.; Tkachenko, T.P.; Kuznetsov, A.V.; Kompanets, I.N. In-plane Switching Deformed Helix Ferroelectric Liquid Crystal Display Cells. *Crystals* **2019**, *9*, 543. [CrossRef]
43. Wang, Z.; Servio, P.; Rey, A.D. Pattern formation, structure and functionalities of wrinkled liquid crystal surfaces: A soft matter biomimicry platform. *Front. Soft Matter* **2023**, *3*, 1. [CrossRef]
44. Otón, J.M.; Pereiro-García, J.; Quintana, X.; Caño-García, M.; Otón, E.; Geday, M.A. Optimizing Tunable LC Devices with Twisted Light. *Crystals* **2024**, *14*, 16. [CrossRef]
45. Meier, P.A.; Keuker-Baumann, S.; Röder, T.; Herrmann, H.; Ricken, R.; Silberhorn, C.; Kitzerow, H.S. Optical imaging of ferroelectric domains in periodically poled lithium niobate using ferroelectric liquid crystals. *Opto-Electron. Rev.* **2024**, *32*, e150611. [CrossRef]
46. Dong, R.Y. Advances in NMR studies of liquid crystals. *Annu. Rep. NMR Spectrosc.* **2004**, *53*, 68.
47. Domenici, V. Order and dynamics of rod-like and banana-shaped liquid crystals by H-2 NMR. *Pure Appl. Chem.* **2007**, *79*, 21. [CrossRef]
48. Cifelli, M.; Domenici, V.; Marini, A.; Veracini, C.A. NMR studies of the ferroelectric SmC* phase. *Liq. Cryst.* **2010**, *37*, 935–948. [CrossRef]
49. Domenici, V. The role of NMR in the study of partially ordered materials: Perspectives and challenges. *Pure Appl. Chem.* **2011**, *83*, 67. [CrossRef]
50. Cifelli, M.; Domenici, V.; Dvinskikh, S.V.; Veracini, C.A.; Zimmermann, H. Translational self-diffusion in the smectic phases of ferroelectric liquid crystals: An overview. *Phase Transit.* **2012**, *85*, 861–871. [CrossRef]
51. Cifelli, M.; Domenici, V.; Veracini, C.A. Recent advancements in understanding thermotropic liquid crystal structure and dynamics by means of NMR spectroscopy. *Curr. Opin. Colloid Interface Sci.* **2013**, *18*, 190. [CrossRef]
52. Dong, R.Y. Recent NMR Studies of Thermotropic Liquid Crystals. In *Annual Reports on NMR Spectroscopy*; Webb, G.A., Ed.; Academic Press: Oxford, UK, 2016; Volume 87, p. 41.
53. Saupe, A.; Englert, G. High-resolution nuclear magnetic resonance spectra of orientated molecules. *Phys. Rev. Lett.* **1963**, *11*, 462–464. [CrossRef]
54. Lohman, J.A.B.; MacLean, C. Alignment effects on high resolution NMR spectra, induced by the magnetic field. *Chem. Phys.* **1978**, *35*, 269–274. [CrossRef]
55. Dong, R.Y. *Nuclear Magnetic Resonance of Liquid Crystals*; Springer: New York, NY, USA, 1997; ISBN 978-1-4612-1954-5.
56. Veracini, C.A. *NMR Spectra in Liquid Crystals*; Emsley, J.W., Ed.; NATO ASI Series, Series C, 141; Reidel: Dordrecht, The Netherland, 1985; Chapter 5.
57. Domenici, V.; Geppi, M.; Veracini, C.A. NMR in chiral and achiral smectic phases: Structure, orientational order and dynamics. *Prog. Nucl. Magn. Reson. Spectrosc.* **2007**, *50*, 1–50. [CrossRef]
58. Catalano, D.; Chiezzi, L.; Domenici, V.; Geppi, M.; Veracini, C.A. Study of the Ferroelectric Liquid Crystal 11EB1M7 by Means of $^{2}$H NMR. *J. Phys. Chem. B* **2003**, *107*, 10104–10113. [CrossRef]
59. Catalano, D.; Chiezzi, L.; Domenici, V.; Galli, G.; Veracini, C.A. $^{2}$H NMR Study of a Deuterium Labelled Ferroelectric Liquid-Crystalline Polysiloxane. *Mol. Cryst. Liq. Cryst.* **2003**, *398*, 127–136. [CrossRef]
60. Catalano, D.; Domenici, V.; Marini, A.; Veracini, C.A.; Bubnov, A.; Glogarova, M. Structural and Orientational Properties of the Ferro, Antiferroelectric, and Re-entrant Smectic C* Phases of ZLL7/* by Deuterium NMR and Other Experimental Techniques. *J. Phys. Chem. B* **2006**, *110*, 16459–16470. [CrossRef]
61. Chen, A.; Poon, C.-D.; Dingemans, T.J.; Samulski, E.T. Ferroelectric liquid crystals derived from isoleucine II. Orientational ordering by carbon-13 separated local field spectroscopy. *Liq. Cryst.* **1998**, *24*, 255. [CrossRef]
62. Yoshizawa, A.; Kikuzaki, H.; Fukumasa, M. Microscopic organization of molecules in smectic A and chiral (racemic) smectic C phases: Dynamic molecular deformation effect on the SA to SC∗ (SC) transition. *Liq. Cryst.* **1995**, *18*, 351. [CrossRef]
63. Zhang, J.; Domenici, V.; Dong, R.Y. $^{13}$C NMR study of orientational ordering in smectic A phase of chiral liquid crystals. *Chem. Phys. Lett.* **2007**, *441*, 237–244. [CrossRef]
64. Dong, R.Y.; Geppi, M.; Marini, A.; Hamplova, V.; Kaspar, M.; Veracini, C.A.; Zhang, J. Orientational order of a liquid crystal with three chiral centers by a combined $^{13}$C NMR and DFT approach. *J. Phys. Chem. B* **2007**, *111*, 9787–9794. [CrossRef]
65. Reddy, M.K.; Boopathi, A.A.; Lobo, N.P.; Ramanathan, K.V.; Narasimhaswamy, T. $^{13}$C NMR investigations and order parameters of rod-like molecules with terminal phenyl and thiophene rings in mesogenic core. *J. Magn. Reson. Open* **2022**, *10–11*, 100055. [CrossRef]
66. Sebastiao, P.J.; Cruz, C.; Ribeiro, A.C. Advances in Proton NMR Relaxometry in Thermotropic Liquid Crystals. In *Nuclear Magnetic Resonance Spectroscopy of Liquid Crystals*; Dong, R.Y., Ed.; World Scientific Co.: London, UK, 2009; pp. 129–167.
67. Ferraz, A.; Zhang, J.; Sebastiao, P.J.; Ribeiro, A.C.; Dong, R.Y. Proton and deuterium nuclear spin relaxation study of the SmA and SmC* phases of BP8Cl-d17: A self-consistent analysis. *Magn. Reson. Chem.* **2014**, *52*, 546–555. [CrossRef] [PubMed]

68. Apih, T.; Domenici, V.; Gradisek, A.; Hamplova, V.; Kaspar, M.; Sebastiao, P.J.; Vilfan, M. 1H NMR Relaxometry Study of a Rod-Like Chiral Liquid Crystal in Its Isotropic, Cholesteric, TGBA*, and TGBC* Phases. *J. Phys. Chem. B* **2010**, *114*, 11993–12001. [CrossRef] [PubMed]
69. Cifelli, M.; McDonald, P.J.; Veracini, C.A. Translational self-diffusion in 4-n-octyloxy-4′-cyanobiphenyl (8OCB) exploited with a static field gradient $^{1}$H NMR diffusometry approach. *Phys. Chem. Chem. Phys.* **2014**, *6*, 4701–4706. [CrossRef]
70. Cifelli, M.; Veracini, C.A. Translational Diffusion in Thermotropic Smectic Phases. *Mol. Cryst. Liq. Cryst.* **2013**, *576*, 127–134. [CrossRef]
71. Cifelli, M.; Domenici, V.; Dvinskikh, S.V.; Glogarova, M.; Veracini, C.A. Translational self-diffusion in the synclinic to anticlinic phases of a ferroelectric liquid crystal. *Soft Matter* **2010**, *6*, 5999–6003. [CrossRef]
72. Kneppe, H.; Reiffenrath, V.; Schneider, F. Anisotropy of the magnetic susceptibility of some nematic liquid crystals. *Chem. Phys. Lett.* **1982**, *87*, 59–62. [CrossRef]
73. Muševic, I.; Blinc, R.; Zekš, B. *The Physics of Ferroelectric and Antiferroelectric Liquid Crystals*; World Scientific Publishing Co.: Singapore, 2000.
74. Zalar, B.; Gregorovič, A.; Simsič, M.; Zidanšek, A.; Blinc, R.; Keast, S.; Neubert, M. Anisotropy of the Critical Magnetic Field in a Ferroelectric Liquid Crystal. *Phys. Rev. Lett.* **1998**, *80*, 4458. [CrossRef]
75. Catalano, D.; Cifelli, M.; Domenici, V.; Fodor-Csorba, K.; Richardson, R.; Veracini, C.A. $^{2}$H-NMR and SAXS of a ferroelectric liquid crystal: Unwinding of the ferroelectric chiral helix by high magnetic fields. *Chem. Phys. Lett.* **2001**, *346*, 259–266. [CrossRef]
76. Domenici, V.; Marini, A.; Veracini, C.A.; Zhang, J.; Dong, R.Y. Effect of the magnetic field on the supramolecular structure of chiral smectic C phases: $^{2}$H NMR studies. *ChemPhysChem* **2007**, *8*, 2575–2587. [CrossRef]
77. Nonnenmacher, D.; Jagiella, S.; Song, Q.X.; Lemieux, R.P.; Giesselmann, F. Orientational fluctuations near the smectic A to smectic C phase transition in two "de Vries"-type liquid crystals. *ChemPhysChem* **2013**, *14*, 2990–2995. [CrossRef]
78. Roberts, J.C.; Kapernaum, N.; Song, Q.; Nonnenmacher, D.; Ayub, K.; Giesselmann, F.; Lemieux, R.P. Design of Liquid Crystals with "de Vries-like" Properties: Frustration between SmA- and SmC-Promoting Elements. *J. Am. Chem. Soc.* **2010**, *132*, 364–370. [CrossRef] [PubMed]
79. Bubnov, A.; Kašpar, M.; Novotná, V.; Hamplová, V.; Glogarová, M.; Kapernaum, N.; Giesselmann, F. Effect of lateral methoxy substitution on mesomorphic and structural properties of ferroelectric liquid crystals. *Liq. Cryst.* **2008**, *35*, 1329–1337. [CrossRef]
80. Kaur, S.; Barthakur, A.; Mohiuddin, G.; Guta, S.P.; Dhara, S.; Pal, S.K. Observation of "de Vries-like" properties in bent-core molecules. *Chem. Sci.* **2022**, *13*, 2249–2257. [CrossRef] [PubMed]
81. Swaminathan, V.; Panov, V.P.; Panov, A.; Rodriguez-Lojo, D.; Stevenson, P.J.; Gorecka, E.; Vij, J.K. Design and electro-optic investigations of de Vries chiral smectic liquid crystals for exhibiting broad temperature ranges of SmA* and SmC* phases and fast electro-optic switching. *J. Mater. Chem. C* **2020**, *8*, 4859–4868. [CrossRef]
82. Schulz, F.; Lutz, B.; Rueck, D.; Batman, D.; Frey, W.; Laschat, S. Tailoring liquid crystalline self-assembly and de Vries behavior of azulenes via lateral and core substitution. *Soft Matter* **2023**, *19*, 2397–2406. [CrossRef]
83. Poll, K.; Sims, M.T. Sub-layer rationale of anomalous layer-shrinkage from atomistic simulations of a fluorinated mesogen. *Mater. Adv.* **2022**, *3*, 1212–1223. [CrossRef]
84. Marchetti, A.; Domenici, V.; Novotna, V.; Lelli, M.; Cifelli, M.; Lesage, A.; Veracini, C.A. Direct Measure of the Tilt Angle in de Vries-Type Liquid Crystals through NMR Spectroscopy. *ChemPhysChem* **2010**, *11*, 1641–1645. [CrossRef] [PubMed]
85. Domenici, V.; Cifelli, M.; Marchetti, A.; Lelli, M.; Hamplova, V.; Kaspar, M.; Veracini, C.A. Smectic A-Smectic C* Transition in a "de Vries" Liquid Crystal by $^{2}$H NMR. *Mol. Cryst. Liq. Cryst.* **2012**, *553*, 103–110. [CrossRef]
86. Domenici, V.; Lelli, M.; Cifelli, M.; Hamplova, V.; Marchetti, A.; Veracini, C.A. Conformational Properties and Orientational Order of a de Vries Liquid Crystal Investigated through NMR Spectroscopy. *ChemPhysChem* **2014**, *15*, 1485–1495. [CrossRef]
87. Yoon, H.G.; Agra-Kooijman, D.M.; Ayub, K.; Lemieux, R.P.; Kumar, S. Direct Observation of Diffuse Cone Behavior in de Vries Smectic-A and -C Phases of Organosiloxane Mesogens. *Phys. Rev. Lett.* **2011**, *106*, 087801. [CrossRef]
88. Marini, A.; Domenici, V. $^{2}$H, $^{13}$C NMR and Ab Initio Calculations Applied to the SmC* Phase: Methodology and Case Studies. *Ferroelectrics* **2010**, *395*, 46–59. [CrossRef]
89. Yoshizawa, A.; Kikuzaki, H.; Hirai, T.; Yamane, M. C-13 NMR Observation of molecular motions at the smecticA-smecticC* transition in a racemic (chiral) smectic liquid crystal. *Jpn. J. Appl. Phys.* **1990**, *29*, L1153–L1156. [CrossRef]
90. Yoshizawa, A.; Nishiyama, I.; Kikuzaki, H.; Ise, N. C-13 NMR and X-ray investigations of phase transitions in an antiferroelectric liquid crystal. *Jpn. J. Appl. Phys.* **1992**, *31*, L860–L863. [CrossRef]
91. Sarmento, S.; Chaves, M.R.; Carvalho, P.S.; Nguyen, H.T. Experimental study of a SmA*-SmCA* phase transition. *Liq. Cryst.* **2001**, *28*, 1561–1571. [CrossRef]
92. Photinos, D.J.; Samulski, E.T. On the Origins of Spontaneous Polarization in Tilted Smectic Liquid Crystals. *Science* **1995**, *270*, 783–786. [CrossRef]
93. Gradisek, A.; Domenici, V.; Apih, T.; Novotna, V.; Sebastiao, P.J. $^{1}$H NMR Relaxometric Study of Molecular Dynamics in a "de Vries" Liquid Crystal. *J. Phys. Chem. B* **2016**, *120*, 4706–4714. [CrossRef]
94. Domenici, V.; Marini, A.; Veracini, C.A.; Malanga, C.; Menicagli, R. From the SmA to the Hexatic, Including the SmC*, SmC*$_{A}$ and SmC*re Phases: A $^{2}$H NMR Relaxation Study. *ChemPhysChem* **2009**, *10*, 2679–2691. [CrossRef]

95. Domenici, V.; Geppi, M.; Veracini, C.A.; Zakharov, A.V. Molecular Dynamics in the Smectic A and C* Phases in a Long-Chain Ferroelectric Liquid Crystal: $^{2}$H NMR, Dielectric Properties, and a Theoretical Treatment. *J. Phys. Chem. B* **2005**, *109*, 18369–18377. [CrossRef]
96. Marini, A.; Domenici, V. Conformational Changes at Mesophase Transitions in a Ferroelectric Liquid Crystal by Comparative DFT Computational and $^{13}$C NMR Study. *J. Phys. Chem. B* **2010**, *114*, 10391–10400. [CrossRef]
97. Blinc, R.; Zalar, B.; Gregorovic, A.; Simsic, M.; Zidansek, A.; Neubert, M. Interlayer exchange effects in the deuteron NMR of ferroelectric and antiferroelectric liquid crystals. *Ferroelectrics* **2000**, *45*, 1–5. [CrossRef]
98. Zalar, B.; Gregorovic, A.; Blinc, R. Interlayer molecular exchange in an anticlinically ordered chiral liquid crystal. *Phys. Rev. E* **2000**, *62*, R37–R40. [CrossRef] [PubMed]
99. Xu, J.; Veracini, C.A.; Dong, R.Y. Interlayer jump diffusion in the smectic-C*$_{A}$ phase by angular-dependent $^{2}$H NMR study. *Phys. Rev. E* **2005**, *72*, 051703. [CrossRef] [PubMed]
100. Yoshizawa, A.; Nishiyama, I.; Kikuzaki, H.; Ise, N. The effect of molecular structure on molecular dynamics and ordering in a chiral smectic liquid crystal. *Liq. Cryst.* **1993**, *14*, 513–523. [CrossRef]
101. Satoh, H.; Hiraoka, K.; Uematsu, Y. Molecular dynamics of a chiral smectic, liquid crystal as studied by $^{13}$C NMR spectroscopy. *Ferroelectrics* **1998**, *12*, 99–106. [CrossRef]
102. Catalano, D.; Cifelli, M.; Fodor-Csorba, K.; Gàcs-Baitz, E.; Geppi, M.; Jàkli, A.; Veracini, C.A. Microscopic organization and tilt angle in smectic A and chiral smectic C phases: Characterization and orientational order by $^{2}$H NMR and electric polarization measurements. *Mol. Cryst. Liq. Cryst.* **2000**, *351*, 245–257. [CrossRef]
103. Kubo, C.; Yoshida, S.; Takanishi, Y.; Ishikawa, K.; Takezoe, H. Different Molecular Conformations in Ferroelectric and Antiferroelectric Liquid Crystals Studied by $^{19}$F-NMR Spectroscopy. *Jpn. J. Appl. Phys.* **2002**, *41*, 6080. [CrossRef]
104. Emelyanenko, A.V. Molecular–Statistical Theory for the Description of Re-Entrant Ferroelectric Phase. *Crystals* **2019**, *9*, 583. [CrossRef]
105. Cifelli, M.; Domenici, V.; Veracini, C.A. From the Synclinic to the Anticlinic Smectic Phases: A Deuterium NMR and Diffusion NMR Study. *Mol. Cryst. Liq. Cryst.* **2005**, *429*, 167–179. [CrossRef]
106. Domenici, V.; Marini, A.; Menicagli, R.; Veracini, C.A.; Bubnov, A.; Glogarova, M. Dynamic behaviour of a ferroelectric liquid crystal by means of Nuclear Magnetic Resonance and Dielectric Spectroscopy. *Proc. SPIE—Int. Conf. Opt. Opto Electron.* **2007**, *6587*, F1–F13.